2010

Multifunctional Polymer Synthesis and Incorporation of Gadolinium Compounds and Modified Tungsten Nanoparticles for Improvement of Radiation Shielding for use in Outer Space

Emily Grace Harbert
College of William & Mary - Arts & Sciences

Multifunctional Polymer Synthesis and Incorporation of Gadolinium Compounds and Modified Tungsten Nanoparticles for Improvement of Radiation Shielding for Use in Outer Space

Emily Grace Harbert

Williamsburg, Virginia

Bachelor of Science, The College of William and Mary, 2008

A Thesis presented to the Graduate Faculty
of the College of William and Mary in Candidacy for the Degree of
Master of Science

Department of Chemistry

The College of William and Mary
January 2010

APPROVAL PAGE

This Thesis is submitted in partial fulfillment of
the requirements for the degree of

Master of Science

Emily G. Harbert

Emily Grace Harbert

Approved by the Committee, November 2009

Robert A. Orwoll

Committee Chair
Professor Robert Orwoll, Chemistry
The College of William and Mary

Richard L. Kiefer

Professor Emeritus Richard Kiefer, Chemistry
The College of William and Mary

Robert A. Pike

Professor Robert Pike, Chemistry
The College of William and Mary

Eugene C. Aquino

Dr. Eugene Aquino
International Scientific Technologies, Inc.

ABSTRACT PAGE

Current radiation shielding technology is not effective, except in the short term, for shielding humans from many radiation sources in outer space, such as galactic cosmic radiation, neutrons, and high energy electromagnetic radiation. A new, lightweight shielding material must, therefore, be developed that is both effective and functional against the most dangerous forms of outer space radiation. Both polyimides and poly(arylene ethers) have space compatible properties and allow for modifications that could yield the creation of a new radiation shielding material.

In this research, two different types of polyimides and six different types of poly(arylene ethers) were synthesized and characterized. Modified tungsten nanoparticles were incorporated into polyimides and gadolinium salts were synthesized for incorporation into poly(arylene ethers) in order to strengthen the polymers' shielding capabilities. All of the polymers synthesized have high glass transition temperatures, indicating their suitability for use in outer space. The incorporation of the tungsten or gadolinium compounds did not appear to affect any of the glass-transition temperatures. Furthermore, the glass transition temperatures of the different poly(arylene ether) films can be rationalized in terms of their molecular structure, and the glass transition temperatures of poly(arylene ethers) can be adjusted by synthesizing either a polymer with the correct ratio of monomers or mixing pure polymers to attain the preferred ratio.

TGA results show that all of the polymer films synthesized in this research are thermally stable at high temperatures, and that neither the modified tungsten or the gadolinium phenylacetate had much impact on the thermal properties of the film.

Tensile testing confirms that the polymers synthesized in this research have similar maximum loads and elastic moduli as Kapton, a widely used, commercially available polymer.

This study showed that the tungsten additive did not contribute greatly to the shielding of X-rays by the polyimides. X-ray and neutron absorption testing with poly(arylene ethers), however, revealed that the addition of gadolinium compounds greatly enhanced the radiation shielding capabilities of the polymer.

The methodology and characterization used in this research has furthered an understanding of radiation protection technology and has led to the creation of new materials. These new materials have properties making them suitable for use in outer space and provide enhanced protection against space radiation.

Table of Contents

List of Figures iii
List of Tables iv
Acknowledgements and Funding v

I. Introduction 1
  a. Types of Radiation and Its Risks 2
    i. Galactic Cosmic Radiation 2
    ii. High Energy Electromagnetic Radiation 3
    iii. Neutrons 4
II. Proposed Solution 5
III. Polyimides 7
  a. Background Research 7
    i. Properties 7
    ii. Synthetic Method 8
    iii. Monomers 11
    iv. Benzyl Mercapton Modified Tungsten 12
  b. Experimental Procedures 14
    i. Polyimide Synthesis 14
    ii. Benzyl Mercapton Modified Tungsten Preparation 15
    iii. Thin Film Preparation 16
  c. Characterization 17
    i. Qualitative Sample Characterization 17
    ii. Thermogravimetric Analysis 17
    iii. Differential Scanning Calorimetery 18
    iv. X-Ray Absorption Testing 18
  d. Discussion and Results 20
    i. Polymerizations and Film Preparation 20
    ii. Characterization- TGA and DSC 21
    iii. Characterization- X-Ray Absorption Testing 22
IV. Poly(arylene ethers) 24
  a. Background Research 24
    i. Properties 24
    ii. Synthetic Method 25
    iii. Monomers 28
    iv. Gadolinium Phenylacetate 30
  b. Experimental Procedure 31
    i. Poly(arylene ether) Synthesis 31
    ii. Polymer Purification 33
    iii. Gadolinium Phenylacetate Synthesis 34
    iv. Sample Preparation 35
      1. Thin Films 35
      2. Thick Samples 36
  c. Characterization 39

i. Viscosity 39
ii. Sample Qualitative Characterization 40
iii. Thermogravimetric Analysis 41
iv. Differential Scanning Calorimetery 42
v. Tensile Testing 42
vi. X-Ray Absorption Testing 43
vii. Neutron Absorption Testing 43
d. Gadolinium Phenylacetate Characterization 47
i. Thermogravimetric Analysis 47
ii. Elemental Analysis 48
e. Results and Characterization 48
i. Polymerizations 48
ii. Polymer Purifications and Polymer Solutions 49
iii. Gadolinium Salt Synthesis 51
iv. Film Preparation 52
v. Thick Sample Preparation 54
vi. Polymer Characterization- Viscosity 55
vii. Polymer Characterization- TGA 57
viii. Polymer Characterization-DSC 58
ix. Polymer Characterization- Tensile Testing 61
x. Polymer Characterization- X-Ray Absorption Testing 64
xi. Polymer Characterization- Neutron Absorption Testing 66
V. Conclusions 69

References 72

Appendix I: Film rating system 74
Appendix II: Index of all polyimide films including rating, TGA, and DSC data 75
Appendix III: Example TGA graph 76
Appendix IV: Example DSC graph 77
Appendix V: Polyimide x-ray absorption Beer's law analysis graph 78
Appendix VI: Polyimide X-ray data 79
Appendix VII: Index of all poly(arylene ether) films including rating, TGA, and DSC data 80
Appendix VIII: Poly(arylene ether) thick samples and curing procedures 82
Appendix IX: Poly(arylene ether) viscosity data 85
Appendix X: Poly(arylene ether) Tensile Testing Data 86
Appendix XI: Poly(arylene ether) x-ray absorption data 87
Appendix XII: Poly(arylene ether) x-ray absorption Beer's law analysis graphs 88
Appendix XIII: Poly(arylene ether) neutron absorption data 92
Appendix XIV: Poly(arylene ether) neutron absorption Beer's law analysis graphs 93
Appendix XV: TGA of gadolinium phenylacetate 96

Vita 97

List of Figures

Figure One: Generic form of a hetrocyclic polyimide 7
Figure Two: General synthetic route of polyimides 8
Figure Three: Mechanism for poly(amic acid) formation 8
Figure Four: Thermal Imidization of poly(amic acid) to polyimide 10
Figure Five: Generic diamine with modifiable M core 11
Figure Six: Structure of benzyl mercapton 13
Figure Seven: Representation of benzyl mercaptan modified tungsten 13
Figure Eight: Polyimide polymerization set-up 15
Figure Nine: Modified Beer's law equations to analyze films with varying amounts of tungsten 20
Figure Ten: Generic Structure of a poly(arylene ether 24
Figure Eleven: General method of nuclephillic substitution of a poly(arylene ether) 25
Figure Twelve: Two-step mechanism of nucleophillic substitution 26
Figure Thirteen: Generic bisphenol with modifiable M group 28
Figure Fourteen: Gadolinium phenylacetate 30
Figure Fifteen: Synthetic route of a gadolinium salt 30
Figure Sixteen: Poly(arylene ether) polymerization set-up 32
Figure Seventeen: Viscosity Related Equations 40
Figure Eighteen: Neutron production of Am/Be source and the reaction of In with a neutron 44
Figure Nineteen: Am/Be radiation source contained in polyethylene cylinder with In foil contained in film sample 45
Figure Twenty: Equations relating to In radioactivity 46
Figure Twenty-one: Graph of ln(recorded counts) versus time for a pure p-HPB/BPF film 47
Figure Twenty-two: Graph of glass transition temperature vs. % p-HPB monomer 60
Figure Twenty-three: Diagram of how inside of the clamp was roughed 62
Figure Twenty-four: Structure of Kapton 63
Figure Twenty-five: Beer's Law analysis for X-ray absorption for *m*-HPB/BPF 65
Figure Twenty-six: Graph of the percentage of x-rays absorbed vs. wt-% Gd for each of the poly(arylene ethers) 66

List of Tables

Table I: Structures, names and abbreviations of polyimide monomers used 11
Table II: Polyimides synthesized 12
Table III: Melting points of polyimide monomers 14
Table IV: Summary of TGA and DSC results for the polyimides 21
Table V: α and β values for ODA/BTDA and BAM/BTDA 23
Table VI: Structures, names and abbreviations of poly(arylene ether) monomers use 29
Table VII: Poly(arylene ethers) synthesized 29
Table VIII: Total amount of poly(arylene ether) polymers synthesized 34
Table IX: Spindle dimensions 40
Table X: Results of elemental testing by Microlab, Inc. 52
Table XI: Average viscosities of p-HPB/BPF solutions 56
Table XII: Summary of poly(arylene ether) TGA results 57
Table XIII: Summary of poly(arylene ether) DSC results 58
Table XIV: Glass transitions of HPB polymers and HPB polymer mixtures 61
Table XV: X-ray absorption α_p and β values for poly(arylene ethers) 64
Table XVI: X-ray absorption data for poly(arylene ether) thick films 65
Table XVII: Neutron absorption α_p and β values of each polymer type 67

Acknowledgements

First and foremost, I would like to thank Dr. Orwoll for his continued patience, persistence, and understanding. Without him, none of this research would have been possible. I would like to thank Dr. Kiefer for his advice and taking his time to help me with the neutron source, Dr. Pike for his patience in helping use the x-ray diffractometer, Dr. Lucy Hue for her help with tensile and viscosity testing, and Dr. Aquino for his ideas, new equipment, and funding. I would also like to thank Mrs. Menges for her problem solving expertise, Norah Bate for her continued support, Jasmine Tutt for her work with polyimides, Ellen Spears for her willingness to always help, and David Hill for his diligent work with the thermal data.

Lastly, I would like to thank my parents, James and Carol Harbert, for all their help, love, and unyielding belief in me.

Funding

This research was supported by International Scientific Technologies, National Aeronautics and Space Administration, and The College of William and Mary.

I. Introduction

a. The Future of Space Travel

In 2004, United States government policy, *Vision for Space Exploration,* expressly includes new goals and objectives for NASA, focusing primarily on "conducting human expeditions to Mars" and "extended lunar habitation" [1]. The propulsion and navigation technology to send orbiters and rovers to Mars already exist, and we know that manned-exploration of the moon has already occurred. So what are the barriers to humans living on the moon or traveling to Mars? Why, five years later, has this program failed to gain traction? Aside from political and financial issues, part of the answer is this: no current technology can sufficiently shield against long-term radiation exposure. Current forms of radiation shielding are suitable only for short-term exposures. The U.S. National Academies Panel released a report that advises NASA to increase funding for space radiation research. The 2008 report states "that lack of knowledge about the biological effects of and responses to space radiation is the single most important factor limiting prediction of radiation risk associated with human space exploration" [2].

Radiation, such as galactic cosmic radiation, neutrons, and high-energy electromagnetic radiation, represents a critical threat to both humans and their equipment. Presently, all human missions must be limited in duration in order to protect the astronauts from overexposure to these types of space radiation. A new, lightweight shielding material must therefore be developed that is both effective and functional against the most dangerous forms of outer space radiation [3], [4], [5].

b. Types of Radiation and Its Risks

i. Galactic Cosmic Radiation

Galactic cosmic radiation (GCR) consists of atomic nuclei that have lost their surrounding electrons in their travel through space. GCR comes from our galaxy or from distant galaxies and, by the time these particles reach earth, they have speeds that in some cases approach that of light. They are highly energetic, charged particles that are composed primarily of the nuclei of hydrogen and helium, with contributions from all other elements particularly those around iron. Those nuclei of iron and those other elements with high atomic numbers, which have a very high kinetic energy, are called HZE particles [6]. Some of these HZE particles have the capacity to completely penetrate the shielding currently in use. The HZE nuclei travel at such high speeds that, when they collide with the nuclei of a shield, the HZE particles split both themselves and the nuclei of the shield. This results in a cascade of nuclear fragments, leading to both shield degradation and, in some cases, radiation levels behind the shield that are greater than the levels in front of the shield [7].

The HZE particles interact with the shielding material in two ways: first, through columbic interactions of the HZE particles with the electrons and nuclei in the shield and, second, through collisions between the HZE nuclei and the nuclei of the shield. Both types of interactions serve to absorb the energy of the HZE particles and can reduce their damaging effects. Shielding, therefore, becomes most effective when the HZE particles are slowed down and thus, their kinetic energy decreased. The energy loss when the incident nucleus interacts with a target nucleus increases with the charge of the nucleus that is hit by the HZE particles. However, the nuclei of all elements other than hydrogen

have neutrons that add mass but do not interact columbically. Consequently, hydrogen serves as the most effective shielding material per unit mass. It has no neutrons. Also, hydrogen has the highest electron density so it is most effective in columbic interactions [7]. Shielding materials with high hydrogen content, therefore, have this advantage.

ii. High Energy Electromagnetic Radiation

High energy electromagnetic (EM) radiation, such as X-rays and gamma rays, are chargeless forms of radiation. High energy EM radiation interacts with a shielding material in three ways. In the photoelectric effect, an atom absorbs the ray and the atom ejects an electron at energy equal to that of the ray minus the binding energy of the electron. The probability of this type of absorption is proportional to the atomic number of the absorbing atom to the fifth power and inversely proportional to the energy of the ray to the 7/2 power. Consequently, this interaction happens most often with an atom with a high atomic number and lower energy X-rays and gamma rays [7], [8].

Compton scattering is a second type of interaction in which the EM radiation interacts with an atom with enough energy to eject an electron and only a part of the energy from the ray is absorbed. Compton scattering results in a lower energy ray which is deflected from its path. The probability of this type of interaction is proportional to the atomic number of the absorbing atom and inversely proportional to the energy of the ray. This type of scattering is the principal mechanism for rays with an intermediate energy [7], [8].

The third type of high energy EM radiation absorption is pair production. In this process, the ray interacts with the electronic field of an absorbing atom's nucleus and the energy of the ray is converted into an electron-positron pair. The probability of this process is proportional to the atomic number of the absorbing element and also the energy of the ray. This process, therefore, occurs most often with higher energy radiation [7], [8].

iii. Neutrons

Neutrons are produced when high energy-particles, such as GCR, collide with other nuclei resulting in fragmentation. Although isolated neutrons are unstable with only a ten-minute half-life, once produced, neutrons are extremely penetrating because they lack any type of charge that might slow them. Some isotopes, such as ^{157}Gd, ^{113}Cd, and ^{10}B, have large neutron-capture cross sections that can neutralize the harmful effects of neutrons. These neutron-capture cross sections increase as the kinetic energy of the neutron decreases [7].

High hydrogen content is an effective means to slow fast moving neutrons. These low velocity neutrons are called thermal neutrons and have high capture cross sections. We therefore start with two known observations. First, hydrogen can decrease the kinetic energy of the neutrons because the neutrons lose energy best in collisions with particles of the same mass. And second, certain isotopes with large neutron capture cross sections can effectively neutralize the harmful effects of neutrons [7], [8].

II. Proposed Solution

The ideal shielding material should have a high hydrogen content in order both to absorb GCR and to slow fast moving neutrons to facilitate their capture by other nuclei. The new material should also contain high concentrations of an element with a high atomic number to absorb high energy EM radiation and a large neutron capture cross section in order to absorb neutrons. Finally, it is also very important that the new shielding material must be lightweight so it can be efficiently transported into space.

High performance polymers are good candidates for shielding in outer space. They can be produced in many forms with low mass while still maintaining structural integrity. They therefore have the potential to reduce launch costs by lessening the weight of the load and serve as effective, long lasting, load-bearing structures or as plumbing in both spacecraft and lunar habitats. High-performance polymers can also be fabricated into many different forms, including fibers to make space suits [9].

Aliphatic polymers would be strong candidates for shielding because of their high hydrogen content. Some aliphatic polymers—for example, polyethylene and polypropylene—have hydrogen concentrations up to .143 moles of hydrogen per gram. They do not, however, have the structural integrity or thermal stability of aromatic polymers. Aromatic polymers are already commonly used in space, but they lack the high hydrogen concentration needed for radiation shielding [10].

The research reported here involves adding hydrogen-containing units to poly(arylene ethers) and polyimides, both of which are high-strength aromatic polymers, to form hybrid systems that have good shielding properties while also possessing good mechanical, chemical, and thermal characteristics.

In addition to a high hydrogen content, the material also should have atoms with a high atomic number and large neutron capture cross section dispersed evenly throughout the polymer at a molecular level in order to absorb high energy EM radiation and to essentially "catch" damaging neutrons. This research focuses on 1) gadolinium for both neutron and EM radiation shielding and 2) tungsten for EM radiation shielding. The shielding material would be most effective if the added metal were dispersed evenly, at a molecular level, throughout the polymer.

III. Polyimides

a. Background Research

i. Properties

Polyimides are high-performance polymers that can be fabricated into films, fibers, and molded products. Aromatic polyimides were initially commercialized to meet the structural demands of the aerospace industry, but have since been used as molecular composites, and have important applications in the electrical and electro-optic industries. They are known for their high thermal stability, high glass-transition temperatures, and resistance to acids, bases, and many organic solvents. These characteristics derive from the aromatic and hetrocyclic rings in the polymer backbone [12], [13], [14].

Figure One shows a generic structure of a polyimide where R is a diamine core. This core is where aliphatic groups can be added to the diamine monomer in order to increase the hydrogen content of the polymer. Hue et al. have already shown that aromatic polyimides can be modified to have up to .056 moles hydrogen per gram [10].

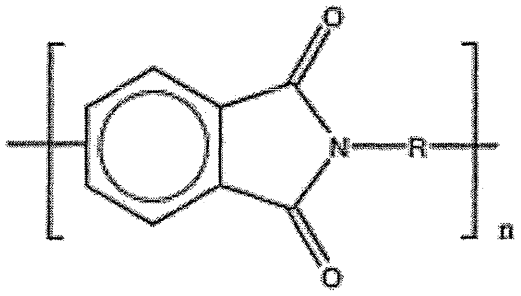

Figure One: Generic form of a hetrocyclic polyimide

ii. Synthetic Method

The easiest and most common synthetic method for producing polyimides begins as a low temperature condensation polymerization in aprotic solvents. The reaction utilizes a dianahydride and a diamine which react at room temperature to form a poly(amic acid). Imidization occurs subsequently when the poly(amic acid) is heated to 300 °C and two molar equivalents of water are removed [13], [14],[15]. The general reaction is shown in Figure Two, and the mechanism for the poly(amic acid) formation is shown in Figure Three.

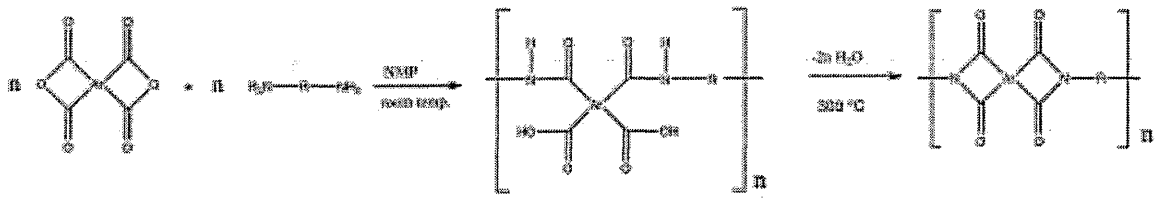

Dianhydride Diamine Poly(amic acid) Polyimide

Figure Two: General synthetic route of polyimides

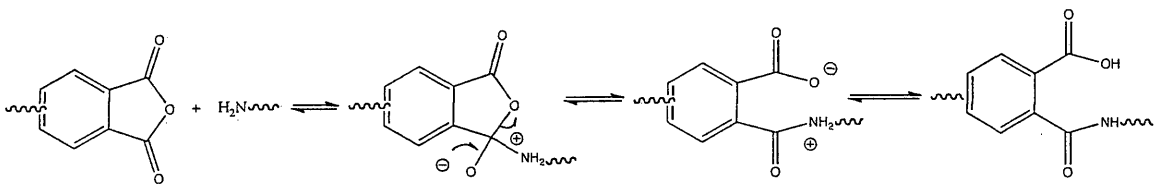

Figure Three: Mechanism for poly(amic acid) formation

It is generally accepted that, the forward reaction begins with a charge-transfer complex between the dianhydride and the diamine. The reaction is then immediately propagated by nucleophilic substitution at one of the dianhydride's carbonyl carbon atoms, where the amine nucleophile attacks the sp^2 carbon [14].

It is important to realize that the formation of the poly(amic acid) is in equilibrium, however, because the first step in the reverse reaction involves a transfer of the carboxyl proton to the adjacent carboxamide group. Any solvent that stops this process can greatly decrease the reverse reaction and force the equilibrium to the right. It is important, therefore, to use a polar, aprotic solvent which will form strong hydrogen bonded complexes with the free carboxyl groups [14].

The reactivity of the monomers is controlled by the electron affinity of the dianhydride and the ionization potential of the diamine. The strongest interactions and best nucleophilic attacks take place when the polyimide is made from a dianhydride with a high electron affinity and a diamine with a low ionization potential. Ignoring these considerations may result in a low molecular weight polymer [15].

Although the reaction between the dianhydride and diamine is fairly simple, water can hydrolyze the amic acid. As the reaction proceeds, the viscosity of the solution reaches a maximum and then decreases over time. When the polymerization begins, there is a large polydispersity of the molar mass with very high weight-average molecular mass, $\overline{M_w}$, being responsible for the high solution viscosity. The reverse reaction leads to an equilibrium and the $\overline{M_w}/\overline{M_n}$ ratio decreases, where $\overline{M_n}$ represents the number-average molecular weight. As this ratio decreases, so does the solution viscosity [15].

Finally, one of the most important considerations must be the stoichiometry of the reactants and the molecular weight control of the final polymer. The highest molecular weights have been found with a 1:1 stoichiometry of the dianhydride and diamine reactants [12]. Careful attention, therefore, is required in order to eliminate impurities in the monomers that might impair and prematurely halt the delicate step-polymerization process. Even the slightest incorrect ratio could cause the premature termination and thus an unsuccessful reaction. It is important to remember that in the step-polymerization process, the desired high molecular weights are only obtained near the end of the reaction. Any early termination of the reaction does not yield a polymer with the desired strength and mechanical properties [13], [14], [15].

While *N*-methyl pyrrolidone (NMP) or *N,N*-dimethylacetamide (DMAc) are the most commonly used solvents, most polar, aprotic solvents that dissolve both monomers can be used [15].

Thermal imidization of the poly(amic acid) occurs at temperature ranges 250-300°. A possible imidization scheme can be found in Figure Four. Imidization is also known to proceed faster in amide solvents because the solvent molecules allow the reactants to arrange into more favorable conformations for cyclization [15].

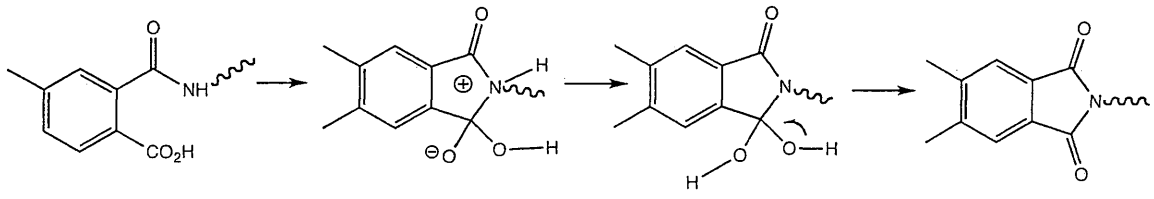

Figure Four: Thermal Imidization of poly(amic acid) to polyimide

iii. Monomers

For this research, BTDA was the dianhydride and ODA and BAM were the diamines chosen. Their chemical names and structures are given in Table I. Modifications to increase the hydrogen content in polyimides depend on the types of monomers used in the synthesis. Figure Five shows the M group of the diamine that is most easily modified. By selecting an M group that includes a high hydrogen-to-carbon ratio, the overall hydrogen content of the polymer is increased. Table II shows the repeat units of all polyimides synthesized.

Figure Five: Generic diamine with modifiable M core

Compound	Name	Abbreviation
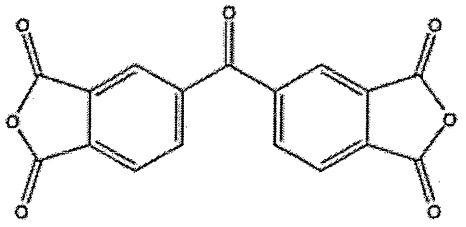	1,2,4,5 Benzenetetracarboxylic dianahydride	BTDA
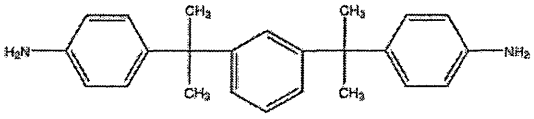	4,4'-(1,3-Phenylenediisopropy-lidene) bisaniline	BAM
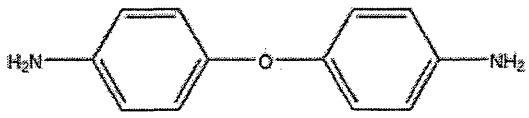	4,4'-Oxydianiline	ODA

Table I: Polyimide monomers used

Polymer Repeat Unit	Name
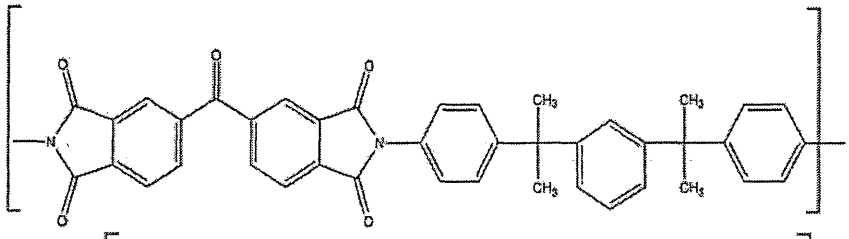	BTDA/BAM
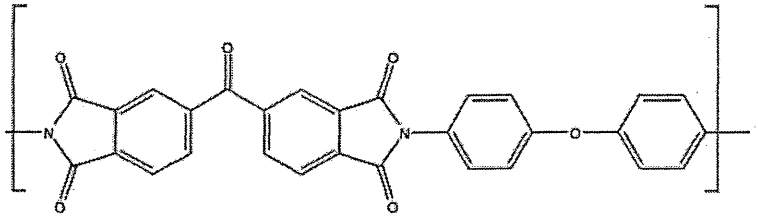	BTDA/ODA

Table II: Polyimides synthesized

i. Benzyl Mercaptan Modified Tungsten

Tungsten is a heavy metal with a high atomic number (Z= 74) that allows it to effectively serve as an EM trap [16].

Tungsten particles or tungsten-based compounds did not dissolve in any of the solvents or polyimides that are being used in this research. Mixing these solids to form a suspension resulted in a very uneven distribution of the nanoparticles throughout the polymer.

Benzyl mercaptan (see Figure Six) was chosen as a modifier to promote the dispersion of the tungsten in the polymer. The thiol group has a lone pair of electrons that interact with tungsten. With these interactions, the thiol group should be able to provide a point of attachment for the benzyl mercaptan to coat the surface of a tungsten

nanoparticle (see Figure Seven). The aromatic nature of the benzyl group renders the tungsten particle more compatible with both the organic polymer and the solvents being used. In this way, a more even distribution of tungsten in the polymer may be achieved [17].

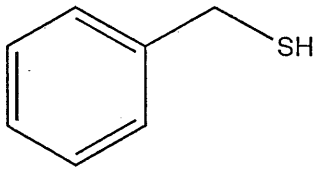

Figure Six: Structure of benzyl mercaptan

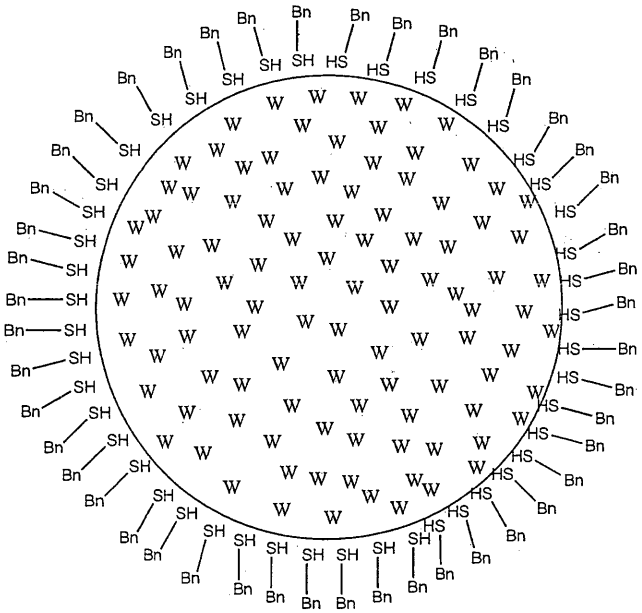

Figure Seven: Representation of benzyl mercaptan modified tungsten

b. Experimental Procedure

i. Polyimide Synthesis

Monomers BTDA, ODA, and BAM were purchased from Sigma-Aldrich. ODA and BAM were recrystallized in ethanol and then dried in an oven at 100°C. BTDA was heated in an oven overnight at 135°C to remove water and ensure that the monomer was not hydrated. The melting points of these monomers after purification were measured with a Mel-Temp instrument and observed to be about 2°C higher than the stock monomer (see Table III). The recrystallization was thus determined to be a necessary step preceding polymerization.

	Stock (°C)	**Recrystallized (°C)**	**Literature Recrystallized (°C) [14]**
ODA	178-180	180-182	181-182
BAM	103-105	105-107	107-108

Table III: Melting points of polyimide monomers

Polymerizations were carried out using a 1:1 ratio of the dianahydride BTDA to one of the two diamines, ODA or BAM. The reaction took place in NMP. Both monomers were separately dissolved in NMP to form 15-20 wt.% solutions. The diamine/NMP solution was first added into a three-neck flask (See Figure Six). Then the dianahydride/NMP solution was allowed to drip from an addition funnel into the flask slowly for about an hour. The second neck of the flask was connected to a nitrogen tank to ensure a nitrogen environment that would keep out oxygen and water vapor that could slow or entirely quench the polymerization. The third neck was connected to a drying tube filled with Drierite in order to prevent any moisture from entering the flask. As

nitrogen gas is blown through the flask, any water created in the reaction will be blown through the drying tube. Any excess moisture could cause molecular weight reduction from the hydrolysis of the polyamic acid.

A magnetic stir bar inside the flask mixed the solution, which sat atop a stir plate. The polymerization ran for 20- 24 hours. See Figure Eight for the polymerization set-up.

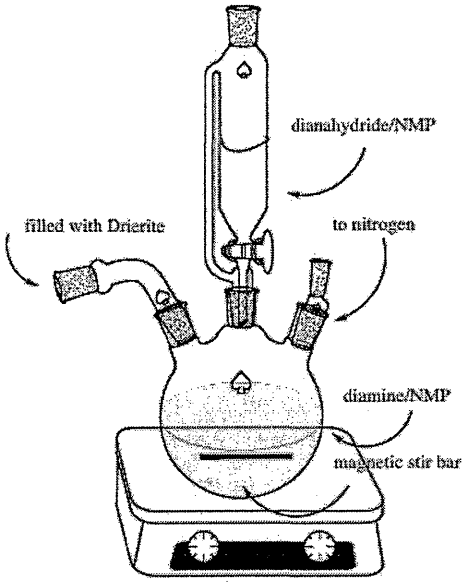

Figure Eight: Polyimide polymerization set-up

As an example, an ODA/BTDA polymer was synthesized by combining 1.9158 grams of ODA in 10.54 mL NMP with 3.0841 grams of BTDA in 15.67 mL NMP.

ii. Benzyl Mercaptan Modified Tungsten Preparation

Both tungsten and benzyl mercaptan were purchased from Sigma-Aldrich. Tungsten nanoparticles were first added to toluene to yield one mole of tungsten per liter of liquid. Benzyl mercaptan was then added to the mixture by syringe for a 1:5 molar

ratio of benzyl mercaptan to tungsten. The mixture was then shaken and allowed to sit for about an hour before it was centrifuged for thirty minutes. The liquid was then decanted and the solid was allowed to dry overnight in an oven at 100 °C.

For example, 0.8857 grams tungsten was added to 4.818 mL of toluene, and then 113.370 μL of benzyl mercaptan was added to the mixture.

iii. Thin Film Preparation

The tungsten, modified with benzyl mercaptan, was added to the poly(amic acid) solution in amounts that would result in a dried film that contained 0, 5, 10, or, 15 wt-% of the element tungsten. After the modified tungsten was added, the mixture was stirred for about twelve hours.

Thin film samples were made on glass plates that had been meticulously cleaned. First, the glass was soaked for about an hour in a potassium hydroxide base bath to eliminate any oily buildup, cleaned with soap and water, rinsed with deionized water, rinsed again with acetone, and rinsed a third time with ethanol to remove the film that acetone leaves when it dries on glass. The glass plate was then set out to dry. As a last measure, hot air from a heat gun was blown over the glass to rid the plate of solvent and dust. Finally, a razor blade was scraped over the entire plate to remove any remaining dust. The glass plates measured 10 inches x 12 inches by 62.5 millimeters.

Films were cast by using a doctor blade with a thickness set to 0.25 mm with one film being made from each poly(amic acid) solution. Each polymer solution was then poured onto a plate along a line near one end of the plate and then the doctor blade was

pulled toward the other end over the line of solution. From here, the films were immediately placed in a programmable oven for thermal imidization. The oven was set to take one hour to ramp up to 100°C, hold a constant temperature at 100°C for one hour, take one hour to ramp up to 200°C, hold a constant temperature at 200°C for one hour, take one hour ramp up to 300°C, and hold a constant temperature at 300°C for one hour.

After the film was removed from the oven, the glass plates were placed in 80°C water until the film could be easily removed. The film was then rinsed with water and ethanol and dried with a paper towel.

c. Characterization

i. Qualitative Sample Characterization

All thin-film samples were qualitatively characterized based on their transparency, amount of bubbles, amount of specks present in the sample, and flexibility. Appendix I describes the film rating system. Appendix II contains all ratings of all polyimide films made.

ii. Thermogravimetric Analysis

All polymer films were tested in a nitrogen environment using a TA Instruments Q500 thermogravimetric analyzer (TGA). This test allowed an analysis of the thermal stabilities of the samples by measuring the mass loss as a function of temperature as the films were heated. About 5 mg of the film was heated to 700 °C at a rate of 10 °C per

minute, with a nitrogen balance purge flow of 40 mL/min and a sample purge flow of 60 mL/min. All of the TGA data from the polyimides can be found in Appendix II. An example of a TGA graph can be found in Appendix III.

iii. Differential Scanning Calorimetry

All of the polymer films were tested in a TA 2920 modulated differential scanning calorimeter (DSC) in a nitrogen environment in order to determine the glass transition temperature of the polymer. Five-milligram samples were tested. The procedure began by equilibrating the temperature at 50°C, raising the temperature to 300°C at a rate of 15°C per minute, and then holding the temperature at 300°C for two minutes. From there, the sample was cooled to 100°C, heated again to 300°C at a rate of 15°C per minute, and then cooled to room temperature. The Tg was found by taking the inflection point of the graph from the second heating. An example DSC graph can be found in Appendix IV.

Individual glass transition temperatures (Tg) obtained from the DSC can be found in Appendix II.

iv. X-Ray Absorption Testing

A Bruker SMART APEX II X-ray defractometer tested the effectiveness of polymer samples in reducing the intensity of X-ray radiation. By covering the X-ray detector, measuring 3 inches by 3 inches, with a polymer film, the known diffraction

peaks of an inorganic crystal, $KMo_2O_5(C_2O_4)(H_2O)_2$, were recorded at constant 2θ values.

To begin, the crystal was mounted 101.900 mm from the detector and underwent a 360° ϕ scan with 2θ=30.000°, ω = 311.000°, and χ = 54.736° with three second exposure times. All images were recorded and examined to find an image with a uniform, high intensity peak. The one degree ϕ range from the chosen image was recorded and ten additional still images were taken, varying the ϕ by .1°. In this way, a strong, known peak was chosen for analysis. For the polyimide testing, a ϕ value of 340.280 was chosen with $2\theta = 27.900°$.

For each film that was tested, seven identical still images were taken and the corresponding intensities were analyzed by recording the number of pixels in the peak. These values were then averaged to find the intensity, *I*, of the X-rays that passed through the film. Before and after testing each film, a blank, with nothing covering the detector, was run and the corresponding intensities were recorded and averaged to determine the intensity of the X-ray beam hitting the film, I_o.

According to the Beer-Lambert law, the intensity, *I*, of electromagnetic radiation passing through a homogenous substance decreases exponentially with its thickness (see Equation One, Figure Nine). I_0 represents the intensity of the incident beam on the film and α represents the material's absorption coefficient. For tungsten-containing polyimide films, the absorption coefficient, α, can be written as a linear function of the weight fraction, *c*, of tungsten present in the polymer (see Equation Two, Figure Nine). These two expressions can be combined, where α_p is the absorption coefficient of the

polymer, β is the absorption coefficient that measures the contribution of the included metal to the absorption, and t is the thickness of the film (see Equation Three, Figure Nine). The combined equation can be plotted so that the left side of the equation versus c has a slope of - β and an intercept of - α_p (5). Theoretically, the β value should be the same for all polymers with tungsten. A graph for the polyimides can be found in Appendix V.

$$I(t) = I_0 e^{(-\alpha t)} \qquad \textit{Equation One}$$

$$\alpha = \alpha_p + \beta c \qquad \textit{Equation Two}$$

$$(1/t)\ln\left[I(t)/I_0\right] = -\alpha_p - \beta c \qquad \textit{Equation Three}$$

Figure Nine: Modified Beer's law equations to analyze films with varying amounts of tungsten

In this research, all films and thick samples that were rated a 3 or higher and had 3 inch by 3 inch samples available were tested. The thickness and percentage of X-rays absorbed can be found in Appendix VI. The weight fraction of tungsten varied from 0 to 0.15. Samples of BAM/BTDA and ODA/BTDA were tested.

d. Results and Discussion

i. Polymerizations and Film Preparation

Polymerizations were usually successful. Only one polymerization resulted in a brittle film that did not crease. Solution viscosity was a large obstacle in the polymerizations. In general, 15 wt-% solutions were too runny and resulted in films with

uneven polymer distribution. Polymerizations made with 20 wt-% solutions, however, were too thick and it was difficult to pour the solution from the flask onto the glass plate. Intermediate concentrations (17 wt-%) resulted in solutions that were viscous but still pourable.

ii. Characterization-TGA and DSC

Differential scanning calorimetery measurements and thermogravimetric analyses were all conducted to ensure that the polymerizations had produced the desired polymer and that there was some consistency among the same polymers. Generally speaking, all test results were very good. All of the results can be found in Appendix Two. A summary of the DSC and TGA data can be found in Table IV. Tabulated are the average temperatures at which 10% of the film's mass was lost on heating in a nitrogen atmosphere and the glass transition temperature.

Polymer Type	Average 10% Degradation Temperature (°C)	Average Glass Transition Temperature (°C)
BAM/BTDA	505	217
ODA/BTDA	546	276

Table IV: Summary of TGA and DSC results for the polyimides.

DSC results show that polymer films having the same molecular structure all have similar glass transition temperatures. Furthermore, the glass transition temperatures of the polymer films having different molecular structures can be characterized. Rigid polymers

have higher glass transition temperatures, as their molecular mobility is restricted by the rigidity in the backbone[18]. This is consistent with the DSC results. The ODA/BTDA polymers have higher Tg's as they have a more rigid and extended backbone than BAM/BTDA which has a kink in the polymer chain due its the meta-substitution.

TGA analysis revealed that all the polymers displayed high thermal stability, as shown by the high temperatures for 5% and 10% degradation (see Appendix II). All samples tested were stable in nitrogen up to at least 400°C and many polymer films showed no mass loss until almost 500°C. Furthermore, TGA results show that the solvent had been removed from the films prior to testing, as there were no polymer films that showed mass loss around the boiling point of the solvent NMP. There did seem to be some variation, however, with the 5% mass-loss temperature. The same film was tested multiple times and although the 5% mass-loss temperature varied, the 10% mass-loss temperature remained constant within a few degrees. This can be explained as instrumental irregularities. Therefore, 10% mass loss temperatures are the ones that are reported.

Films that contained the benzyl mercaptan modified tungsten had 10% mass-loss temperatures and glass-transition temperatures similar to those of the pure polyimide films. This indicates that the filler does not affect the film's thermal degradation.

iii. Characterization- X-Ray Absorption Data

Table V shows all polyimide films tested with incident X-rays, including film thickness and the percentage of the incident X-rays that the film has shielded. Pure films

shield only 7% to 8% of the X-rays; films containing 15 wt-% tungsten shielded up to 10% of the X-rays. Tungsten, therefore, does not seen to be an effective additive to shield against high energy EM radiation.

Film ID	% W	3x3 Inch Thickness (mm)	% X-Rays Absorbed
BAMBT-06	0	0.030	7
ODABT-06	0	0.055	8
ODABT-10	5	0.059	10
ODABT-11	10	0.045	9
ODABT-12	15	0.048	10

Table V: X-ray absorption data for ODA/BTDA and BAM/BTDA

Due to film quality, only one BAM/BTDA film could be tested. Appendix V contains the graph of the Beer's law analysis for the ODA/BTDA films, where $\beta = 10\ mm^{-1}$ and $\alpha_p = 78\ mm^{-1}$.

IV. Poly(arylene ethers)

a. Background Research

i. Properties

Poly(arylene ethers) are high performance polymers that that can be made into many different types of films, fibers, and molded pieces. They are known for their resistance to acids, alkalis, and hydrolysis; they exhibit low flammability. Their glass transition temperatures cover a wide range depending on their molecular structure and are generally thermally stable up to at least 350°C [9], [20], [21].

Figure Eight shows a generic structure of a poly(arylene ether), where Y is a bisphenol core. This core is where aliphatic groups can be added to the bisphenol monomer in order to increase the hydrogen content of the polymer. Hue et al. have already shown that poly(arylene ethers) can be synthesized with up to 0.069 moles hydrogen per gram [10].

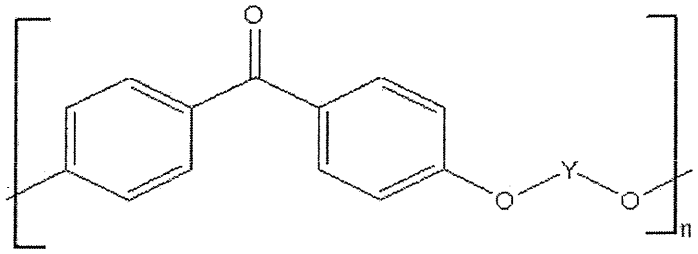

Figure Ten: Generic Structure of a poly(arylene ether)

The aryl C-O-C ether linkage has a lower rotation barrier than the C-C bond; therefore, the C-O-C bond introduces considerable flexibility into the poly(arylene

ether)'s backbone. This allows for greater energy dispersion which is believed to be the main reason for the impact resistance and toughness in poly(arylene ethers) [20].

ii. Synthetic Method

Nucleophillic substitution is the most common synthetic method for poly(arylene ethers) because of the availability of the aromatic dihydroxy and the activated dihalo compounds and the ease of the actual polymerization reaction. The general synthesis of poly(arylene ethers) is shown in Figure Eleven. The two-step reaction mechanism for diphenols and activated aromatic dihalides is shown in Figure Twelve. For the latter reaction, a dihalide, with a halide leaving group, is reacted with a phenylate ion, which is used to replace the halide, thus forming a polymer [9].

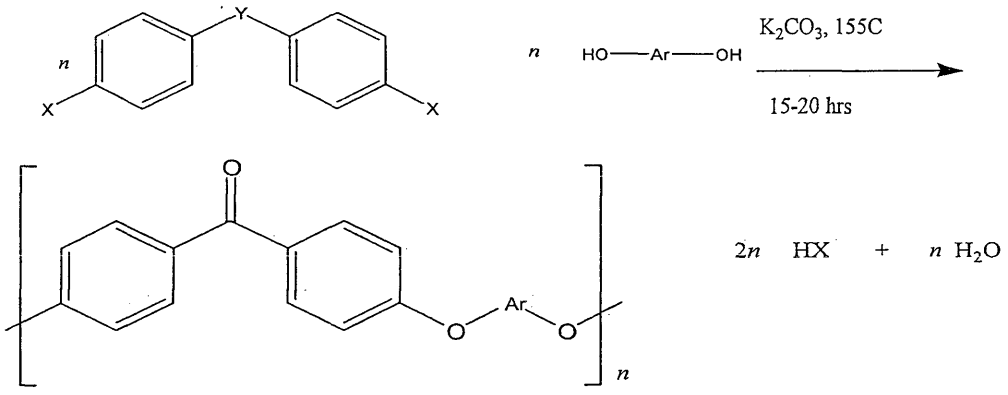

Figure Eleven: General method of nuclephillic substitution of a poly(arylene ether) (X=halogen, Y=bridging atom or group, Ar=aromatic compound)

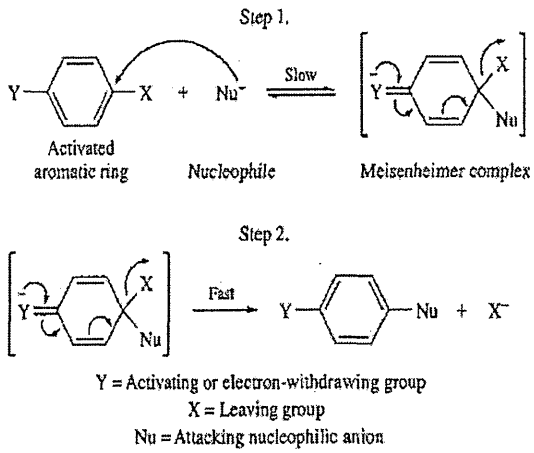

Figure Twelve: Two-step mechanism of nucleophillic substitution [15]

In the first step, a phenylate ion is formed when the bisphenol is deprotonated by the reaction with the carbonate ion. This phenylate, the nucleophile, attacks the carbon of the C-X bond (where X= Cl or F), thus creating a resonance-stabilized intermediate as shown in Figure Twelve. In the next step, the halide leaving group detaches from the intermediate. Just as electron affinity decreases in the order F>>Cl >Br, I, so does the halogen reactivity with the activating group. The order of reactivity of the leaving group can be explained by the increased stabilization of the intermediate by increasing electronegativity through Y's electron withdrawing effects. Furthermore, the carbon directly attached to the halide is more electrophilic and therefore more susceptible to nucleophilic attack. The biggest problem when dealing with the bisphenol is that it has decreasing stability at the temperatures at which the polymerization must occur. Many bisphenols have a tendency to cleave at temperatures above 160 °C, therefore the thermal stability of both the bisphenol and its salt must be examined [9].

Choosing the most suitable electron withdrawing group (represented by Y in Figures Eleven and Twelve) to activate the aromatic group is also important in the polymer synthesis. When common activating groups, such as

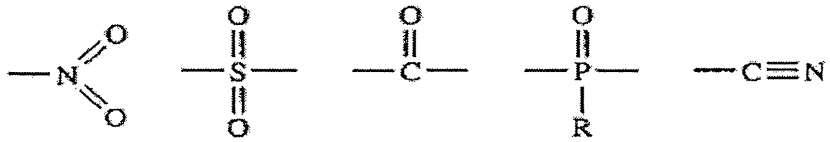

are ortho and para to the leaving group, the rate of the first step of the polymerization increases because they also help stabilize the intermediate. Conversely, electron donating groups such as amines decrease the stability and slow down the reaction rate [9].

When choosing a base for the reaction, potassium carbonate often works better than sodium carbonate and is much more soluble in the polar, aprotic solvents used. Also, the potassium phenoxides that are formed are more reactive than the sodium phenoxides [9].

Toluene is added to the reaction mixture because it forms an azeotrope with water and promotes the removal the water formed from the disproporation of potassium carbonate during the reaction. Additionally, aprotic, polar solvents such as *N,N*-dimethylacetamide (DMAc) or *N*-methyl-2-pyrrolidone (NMP) are commonly used. In any case, it is acceptable to use almost any other aprotic, polar solvent as long as it is thermally stable at the polymerization temperature and it dissolves the poly(arylene ether) [9],[20].

Finally, like polyimides, one of the most important considerations must be the stoichiometry of the reactants and the molecular weight control of the final polymer. The

ideal and highest molecular weights have been found with a 1:1 stoichiometry with the bisphenol and dihalide reactants [9].

iii. Monomers

For this research, BPF was the dihalide and m-HPB, p-HPB, and BPA were the bisphenols chosen. Their chemical names and structures are given in Table VI. Modifications to increase the hydrogen content in poly(arylene ethers) depend on the monomers used in the synthesis. Figure Thirteen shows the M group of the bisphenol that is most easily modified. By selecting an M group that includes a high hydrogen-to-carbon ratio, the overall hydrogen content of the polymer is increased. Table VII shows the repeat unit of all poly(arylene ethers) synthesized.

Another important consideration is the geometry of the monomer. Bisphenols *m*-HPB and *p*-HPB are almost identical, except for the meta or para attachment of the central benzene group. This geometrical difference, however, may result in large differences in the overall properties of the polymer. In this research, these differences will be investigated in order to find the most suitable polymer for space applications.

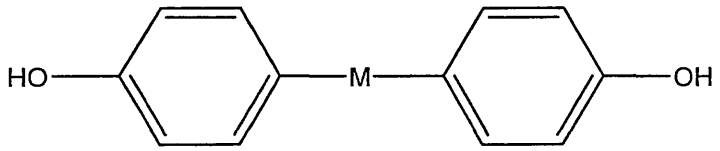

Figure Thirteen: Generic bisphenol with modifiable M group

Compound	Name	Abbreviation
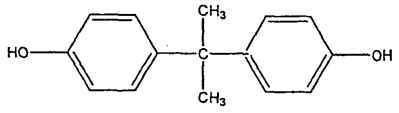	Bisphenol A	BPA
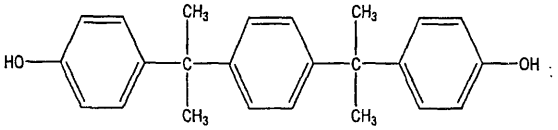	1,4-bis[4-hydroxypheneyl-2-propyl]benzene	*p*-HPB
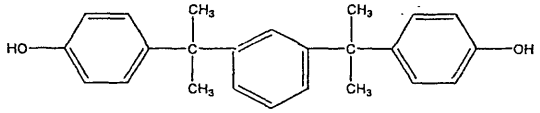	1,3-bis[4-hydroxypheneyl-2-propyl]benzene	*m*-HPB
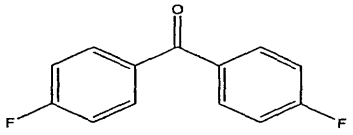	4,4'-difluorobenzophenone	BPF

Table VI: Structures, names and abbreviations of poly(arylene ether) monomers used

Polymer Repeat Unit	Name
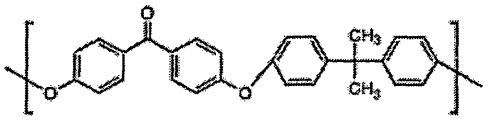	BFA/BPF
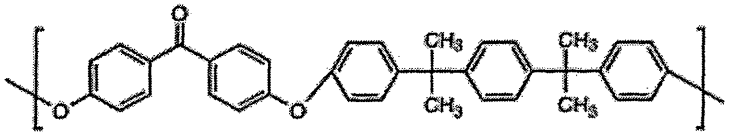	p-HPB/BPF
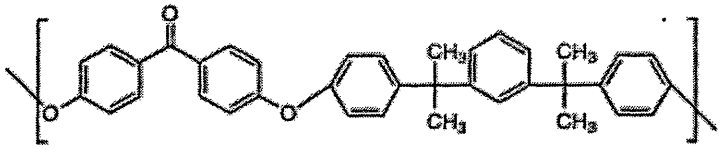	m-HPB/BPF
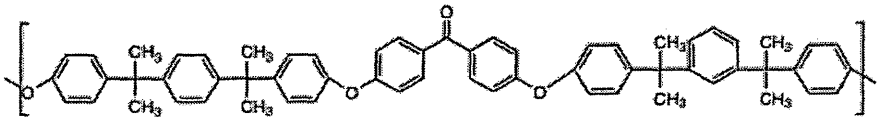	m-HPB/p-HPB/BPF

Table VII: Poly(arylene ethers) synthesized

iv. Gadolinium Phenylacetate

Gadolinium is a heavy metal with both a high atomic number (Z= 64) and a large thermal neutron-capture cross section (σ_n= 49,000 barns/atom). These two features allow it to effectively serve as both a neutron and a high-energy electromagnetic radiation trap [7]. It has already been shown that gadolinium salts can be synthesized from organic acids [22]. Previous research in this lab has shown that gadolinium phenylacetate is soluble in the same solution as the polymer (See Figure Fourteen) [11]. The molecular dispersion of the gadolinium is thus maximized along with its radiation shielding abilities. The synthetic route is shown in Figure Fifteen.

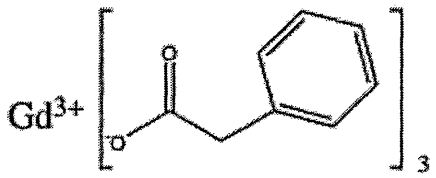

Figure Fourteen: Gadolinium phenylacetate

(1) $Gd(NO_3)_3 + H_2O \longrightarrow Gd^{3+} + 3NO_3^-$

(2) $H\text{-}A + NH_3 \rightleftharpoons NH_4^+ + A^- \rightleftharpoons NH_4\text{-}A + H_2O$

(3) $3A^- + Gd^{3+} \longrightarrow Gd(A)_3$

Figure Fifteen: Synthetic route of a gadolinium salt, where A represents the phenylacetate moity

b. Experimental Procedure

i. Polymer Synthesis

Monomers BPF, BPA, *p*-HPB, and *m*-HPB were purchased from Sigma-Aldrich. Previous research found that the melting points of the recrystallized monomers were, on average, only one degree higher than those of the stock monomers [11]. It was assumed, therefore, that polymers made with the stock monomers would be adequate for the polymerization; recrystallization would be unnecessary.

Polymerizations were carried out using either a 1:1 molar ratio of the dihalide BPF to one of the three bisphenols BPA, *p*-HPB, and *m*-HPB or a 2:1:1 ratio of BPF: *p*-HPB: *m*-HPB. Each reaction took place in a mixture of DMAc and toluene, where the volume of DMAc was determined so that the monomer's mass was 18 wt-% of the final solution, where the amount of toluene used was determined by a 7:3 volumetric ratio of DMAc to toluene. The mass of potassium carbonate, the initiator, was 2.4 times the equimolar mass of potassium carbonate to facilitate the deprotonation of bisphenol monomer. Successive polymerizations had been tested with initiator concentrations of 1.5, 2.0, and 3.0 times the equimolar amount. Subsequently, 2.4x was selected for the concentration of potassium carbonated used in the remaining polymerizations.

Once in the reaction flask, the bisphenol monomer and potassium carbonate were mixed, heated to 60°C and allowed to completely dissolve in the solvent prior to the addition of dihalide monomer in order to allow for the full activation of the bisphenol.

As an example, a *p*-HPB/BPF polymer was synthesized by combining 17.1802 grams of *p*-HPB with 16.4480 grams of potassium carbonate in a solvent mixture

containing 135 mL of DMAc and 58 mL of toluene. Then, 10.8199 grams of BPF were added to begin the polymerization.

All of the components were mixed in a 500-mL, three-neck flask which was positioned in an oil bath. The oil bath sat on a stirrer/hot-plate where both the temperature and the bath stirring rate was controlled. The first neck was connected to a nitrogen tank to ensure a nitrogen environment that would keep out oxygen that could interfere with the polymerization. The middle neck of the flask was connected to a mechanized stir paddle. The third neck held a Dean-Stark trap filled with toluene, attached to a condenser (see Figure Sixteen).

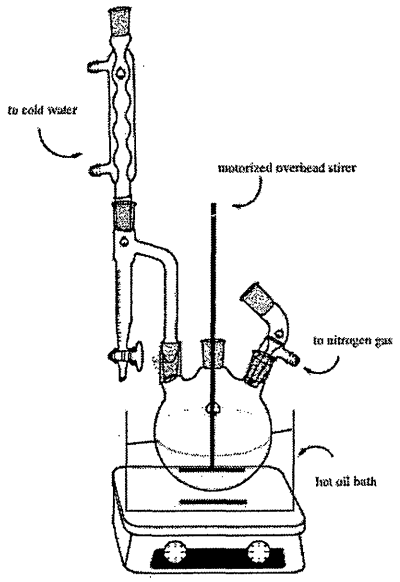

Figure Sixteen: Poly(arylene ether) polymerization set-up

The entire reaction mixture was heated to ca. 165°C and refluxed in a nitrogen environment for 20 to 48 hours. The duration of each polymerization process varied depending on the amount of polymer being produced. Many polymerizations were set up

to yield 28 grams of polymer; these reactions were allowed to run for two days. Smaller batches ran for just under a day. The water byproduct of the polymerization was removed from the resulting mixture as it formed an azeotrope with the low-boiling toluene. Both water and toluene condensed in the condenser. Because water is denser than toluene, the water fell to the bottom of the Dean-Stark trap and displaced the toluene in the liquid layer above it. The displaced liquid toluene ran back into the reaction mixture in a volume equal to the amount of water removed from the system.

After the reaction was completed, the toluene was removed from the reaction system by raising the temperature of the system to ca. 190°C and draining the Dean-Stark trap. A cooling coil was added to the water supply for the condenser in order to cool the water enough for the boiling toluene to condense in the trap. This continued until all of the toluene added to the system was removed.

Throughout the entire polymerization, care was taken to vigilantly monitor the temperature.

ii. Polymer Purification

After cooling the system to about 100 °C, the product mixture was slowly poured into a blender containing a 60:40 volumetric ratio solution of acetic acid and water in order to remove potassium carbonate. Blending and mixing continued until the resulting carbon dioxide bubbles disappeared. The entire solution was then poured into a Büchner funnel, vacuum filtered, washed with boiling deionized water, and then washed again with ethanol. This step was repeated until the smell of acetic acid was no longer present.

The product, consisting of small white polymer pieces, was dried at room temperature overnight.

The polymer was then purified further. The whole process was repeated by dissolving the entire polymer produced in ca. 40mL of NMP, stirring the mixture until the polymer had dissolved, and repeating the blending and filtering. In these additional washings, the polymer was washed five to six times with boiling water in order to completely remove the acetic acid from the polymer. If any acetic acid remained, the polymer turned yellow and hardened into pieces while drying. Most times the entire purification process was repeated up to five times in addition to the initial purification.

The goal of the successive purifications was to achieve a transparent solution when five grams of polymer was dissolved in the solvent to yield a 15% solution. After zero or one purification, the 15% polymer solution was dark yellow and opaque, a probable consequence of lingering acetic acid and potassium carbonate. Table VIII outlines all of the polymerizations and amounts of polymer produced.

Polymer	Number of Polymerizations	Total Grams Produced
p-HPB/BPF	19	510
m-HPB/BPF	17	457
p-HPB/m-HPB/BPF	17	456
BPA/BPF	3	45

Table VIII: Total amount of poly(arylene ether) polymers synthesized

iii. Gadolinium Phenylacetate Synthesis

Gadolinium nitrate and phenylacetic acid were both purchased from Sigma-Aldrich. The gadolinium nitrate was dissolved in about 20 mL of water. The phenylacetic

acid was added to ca. 200 mL of water, although it is not water soluable. Aqueous ammonia was added in drops until the pH of the mixture was between 5 and 6. At this pH, almost all of the phenylacetic acid dissolved. Gadolinium phenylacetate was made by combining the two solutions so that there was a 1:3.2 molar ratio of gadolinium nitrate to deprotonated phenylacetic acid. The gadolinium salt precipitated immediately. The mixture was refrigerated at 0°C overnight. The salt was then vacuum filtered with very fine filter paper, washed with ethanol, and then dried in an oven at 90°C. The gadolinium phenylacetate solid was tested in many common solvents, but was found to be soluble only in DMAc and NMP.

iv. Sample Preparation

Samples were prepared by dissolving the dry polymer in either NMP or DMAc to form solutions that were 15% polymer by weight. If the film was to contain gadolinium phenylacetate, the well-ground salt was added only after the polymer had fully dissolved.

The rotating stir bar tended to cause a bubbling in the solution, so the mixture flask was set into a sonicator for about ten minutes prior to the sample preparation. In later preparations, the mixture was heated to 280°C, cooled, and then centrifuged.

1. Thin Films

Poly(arylene ether) thin films were made in the same manor as the polyimide thin films (see Section III, b, iii).

After each film was pulled, it was placed in a low humidity, tack-free box for about a day, and then placed in a programmable oven. The oven program was the same for films made in NMP (boiling point =202 °C) or DMAc (boiling point = 164°C). The oven was set to take one hour to ramp up to 100°C, hold at 100°C for one hour, take one hour to ramp up to 200°C, hold at 200°C for one hour, take one hour ramp up to 300°C, hold at 300°C for one hour, and then cool to room temperature over a period of two hours. Oven programs, however, that reached a maximum of 250°C were also used.

After the film was removed from the oven, the glass plates were placed in 80°C water until the film could be easily removed. The film was then rinsed with water and ethanol. All poly(arylene ether) films are described in Appendix VII.

2. Thick Samples

In order to produce samples more than a few millimeters thick, several different methods were used.

The first method involved placing a block of aluminum with a square cut out, measuring 3.2 inches long x 3.2 inches wide x 0.5 inches, on top of a glass plate. Solutions of 15% polymer containing about 10 grams polymer were poured onto the glass contained by the aluminum mold. The sample was placed in the dry box and then dried in the oven to remove the solvent. The first attempts resulted in a sample that had bubbled due to the solvent leaving the polymer too quickly. The oven program was adjusted, following a similar procedure, only taking four-and six-hour increments instead of one-hour increments. These samples bubbled severely. The oven program was

adjusted again, to use eight-hour increments. This resulted in a sample that only had one small bubble. These samples were also limited by the relatively small thickness of the mold. After one sample had been fully dried of the solvent, another layer of 15 % polymer solution was poured over the original sample in an attempt to increase its thickness. After one day in the dry box at room temperature, the whole sample had bubbled up above the mold. It seemed that the solvent in the solution permeated the previously dry under-layer and caused massive bubbling of the entire sample.

In each of these attempts, the drying polymer adhered so firmly to the glass plate that, as the sample contracted with the evaporation of the solvent, the glass plate shattered. It was very difficult to separate the sample from the aluminum mold even as pieces of broken glass were removed and even after soaking in hot water as was done with the films. Furthermore, complete removal of the pieces of glass was difficult because the glass had a tendency to break off and stick in slivers to the bottom of the sample.

In the next attempt to prepare thick samples, Pyrex Petri dishes, with a diameter of 3.5 inches and a height of 2.0 inches were used. The dishes were cleaned in the same way as the glass plates. These dishes were improvements over the glass plates and aluminum mold methods as they were deeper and thus allowed for much thicker samples. Samples of these 15% polymer solutions contained up to 20 grams of the polymer. The same oven program that had been used with the glass plate/aluminum mold method was used. All of the samples containing gadolinium made with this method, however, bubbled after being heated in the oven.

A release agent, Sprayon Premium Mold Release Dry Film P.T.F.E., was applied to the inside of the Petri dish in some trials, but this did not aid in the removal of the sample. In order to remove the sample from the dish, the whole apparatus had to be wrapped in paper and the glass broken with a hammer.

The final mold to prepare thick samples involved aluminum dishes measuring 3.8 inches in diameter and 0.8 inches in height, rather than the glass Petri dishes. Samples of 15% polymer contained up to 20 grams of the polymer. The oven program with the 12 hour increments was used again, however, it seemed that only pure samples did not bubble.

A few samples that had bubbled were cut up and placed into a flask with NMP. These sat for over two weeks, but did not dissolve. Instead, the samples seemed to swell and become soft as some solvent was absorbed into the polymer. Next, the flask was placed in the sonicator and a hot water bath, toluene was added, but nothing helped in the dissolution.

A small-scale experiment was then set up in order to determine the temperature at which the bubbles formed. About 1 mL of 15% polymer solution was added to a 5 mL beaker, which was heated on a hot stage. The temperature of the stage was able to reach 150°C before bubbles were formed, although the temperature of the stage was not necessarily the temperature of the polymer solution.

From here, samples were then kept in an oven at 85°C for three days to a week before increasing the temperature. A similar modification to this process was to hold the sample at 85°C under nitrogen, and to cover the sample with a large Petri dish with a small opening and continuing the same curing procedure.

A description of all of the thick samples can be found in Appendix VIII along with all curing processes.

c. Polymer Characterization

i. Viscosity

Viscosity is the measure of internal friction of a fluid. This friction can be measured when one layer of the fluid is made to move in relation to another. The greater the force required to cause this movement, the greater the "shear." Viscosity, η, is defined as the shear stress, τ, divided by the shear rate, γ, (See Figure Seventeen). The viscosity of a polymer solution, therefore, can be determined by measuring the torque required to rotate a spindle, driven by a motor through a calibrated spring, immersed in a solution. For any given viscosity, the resistance to flow—which is given by the degree the spring winds up—is proportional to the spindle's speed of rotation and is related to the spindle's geometry. Newtonian fluids are solutions that have a constant viscosity even as the shear rate is varied. Non-Newtonian fluids are solutions that when the shear rate is varied, the viscosity does not remain constant [23].

Solutions of 15% p-HPB/BPF in NMP were analyzed using a Brookfied DV-E Viscometer, located at AdaptiveEnergy in Hampton Virginia, using a s-18 spindle. Its dimensions can be found in Table IX. The temperature was held constant at 25 °C and the shear rate was varied from 0.6-6.0 RPM. Viscosity measurements were recorded at each shear rate for 0%, 5%, 10%, and 15% Gd and for clear solutions of p-HPB/BPF in NMP. An incompletely polymerized sample was also tested for comparison. Eight-

milliliter samples of each solution were tested. All viscosity data can be found in Appendix IX.

shear rate (sec^{-1}):	$\gamma = \frac{2\omega R_c^2 R_b^2}{x^2\left(R_c^2 - R_b^2\right)}$
shear stress($dynes/cm^2$):	$\tau = \frac{M}{2\pi R_b^{2L}}$
viscosity (poise):	$\eta = \tau/\gamma$
Definitions:	
angular velocity of spindle (rad/sec):	$\omega = (2\pi/N), N = RPM$
radius of container (cm):	R_c
radius of spindle (cm):	R_b
radius at which shear rate is being calculated (cm):	x
torque input by instrument: (dyne-cm):	M
effective length of spindle (cm):	L

Figure Seventeen: Viscosity Related Equations

Spindle	Diameter (mm)	Side Length (mm)	Effective Length (mm)
s-18	17.48	31.72	35.53

Table IX: Spindle dimensions

ii. Sample Qualitative Characterization

All thin film and thick samples were qualitatively characterized based on their transparency, amount of bubbles, amount of specks present in the sample, and flexibility. Appendix I describes the rating system. Appendix VII and Appendix VIII contain all ratings of all thin films and thick samples made.

In addition, films were cut into 3-inch by 3-inch and 1-inch by 1-inch squares for testing. These samples thicknesses were then measured multiple times (seven times for smaller squares and five times for the larger squares). The resulting thicknesses were averaged and can be found in Appendix XI.

iii. Thermogravimetric Analysis

In order to determine the degradation temperature of the film, all polymer films were tested in a thermogravimetric analyzer (TGA) in a nitrogen environment by using a TA Instruments Q500 TGA. This allowed an analysis of the thermal stabilities of the samples by measuring the mass loss as a function of temperature as the films were heated. About 5-mg of each film was heated to 700 °C at a rate of 10 °C per minute, with a balance purge flow of 40 mL/min and a sample purge flow of 60 mL/min. All of the thermal data can be found in Appendix VII.

iv. Differential Scanning Calorimetry

In order to determine the glass transition temperature of the polymer, 5-mg samples of all of the polymer films and many of the thick samples were tested in a TA 2920 modulated differential scanning calorimeter (DSC). The procedure began by equilibrating the temperature at 50°C, raising the temperature to 300°C at a rate of 15°C per minute, and then holding the temperature at 300°C for two minutes. From there, the sample was cooled to 100°C, heated again to 300°C at a rate of 15°C per minute, and then cooled to room temperature.

The Tg was found by taking the inflection point of the graph. All glass-transition temperatures can be found in Appendix VII.

v. Tensile Testing

The strength of the films was tested by using a Lloyd Instruments LTD Materials Testing LRX 2KS Standard Machine, located at AdapativeEnergy in Hampton, Virgina. Film strips with a width of 10.0 mm were mounted between two clamps with an average separation of 6 inches. The instrument applied a tensile force to determine the elastic moduli of the films.

The preload tension was 0.5 N; the test speed was 0.5-inches per minute; the strain for offset yield was 3%. The load had a maximum of 2500 N and a sensitivity of 106.2%. The test ran until the film broke.

The only films tested were those with enough area after radiation absorption testing samples were cut. In some instances, only one or two strips were available for

testing. Many films could not be tested at all. Tensile testing data can be found in Appendix X.

vi. X-Ray Absorption Testing

Poly(arylene ethers) were tested in the same way as the polyimides (see Section III,c,iv). Two different diffraction peaks ($2\theta = 27.900$, $\phi = 340.280$ and $2\theta = 18.580$, $\phi = 158.630$) were used in the poly(arylene ether) testing, however, because the crystal had shifted slightly after the first set of films were tested. The specific peak that was used for each film is noted in Appendix XI.

All films and thick samples tested had a quality rating of 3 or higher and were large enough to yield 3-inch by 3-inch test specimens. The weight fraction of gadolinium varied from 0 to 0.15. Samples of BPA/BPF, m-HPB/BPF, p-HPB/BPF, and m-HPN/p-HPB/BPF were tested. The results can be found in Appendices IX and X.

vii. Neutron Absorption Testing

An americium/beryllium 1 cuire neutron source[1], located at NASA's Langley Research Center, was used in the neutron absorption testing of the polymer films. Americium (Am) is a radioactive element that emits alpha particles. These alpha particles interact with beryllium (Be) to produce neutrons (Figure Eighteen, Equation One and Equation Two) [8].

[1] Note: The Am/Be radioactive source was used only at NASA's Langley Research Center following NASA's specific guidelines for treatment of a radioactive source.

The Am/Be source was contained in a polyethylene solid cylinder with a small hole drilled in the center (see Figure Nineteen). The neutrons that are ejected from the source have energies ranging from 1 million to 10 million electron volts [8]. The hydrogen-rich polyethylene casing serves to slow the neutrons down to around .25 electron volts so that they can be captured by the Gd in the polymer film samples.

$$^{241}_{95}Am_{243} \rightarrow ^{4}_{2}He_{2} + ^{237}_{93}Np_{144} \qquad \textit{Equation One}$$

$$^{4}_{2}He_{2} + ^{9}_{4}Be_{5} \rightarrow \left(^{13}_{6}C_{7}\right)^{*} \rightarrow ^{12}_{6}C_{6} + n \qquad \textit{Equation Two}$$

$$^{115}_{49}In_{68} + n \rightarrow ^{116m}_{49}In_{67} \rightarrow ^{116}_{50}Sn_{66} + e^{-} \qquad \textit{Equation Three}$$

Figure Eighteen: Neutron production of Am/Be source (Equation One and Two) and the reaction of In with a neutron [24]

For neutron absorption testing, a piece of indium metal was taped to the surface of the polyethylene cylinder and left overnight. The neutrons with a low enough energy were then captured by the indium. When the stable In^{115} isotope adds a neutron, it is transformed to the radioactive isotope In^{116m} (half life = 54.29 minutes), which then decomposes to tin with the emission of a beta particle (Figure Eighteen, Equation Three) [8].

After a period of time, less than 24 hours, a steady state was established so that the rate of formation of radioactive In^{115} was equal to its rate of decay [24]. The In sample was then placed in a Geiger counter connected to a SpecTech ST360 Radiation Detector, to record the beta-decay of the metal. Twenty-four runs were recorded. Each run was the collection of counts for 100 seconds, followed by a 200-second break. The background radiation was measured prior to each sequence of measurements and the time

needed to remove the samples from the source and place it in the detector was also recorded.

Polymer samples measuring 1.5 x 1.5 inches were tested by taping the film between the In sample and the neutron source. 0%, 5%, 10%, and 15 wt-% Gd film samples were tested for *m*-HPB/BPF, *p*-HPB/BPF, and *m*-HPN/*p*-HPB/BPF.

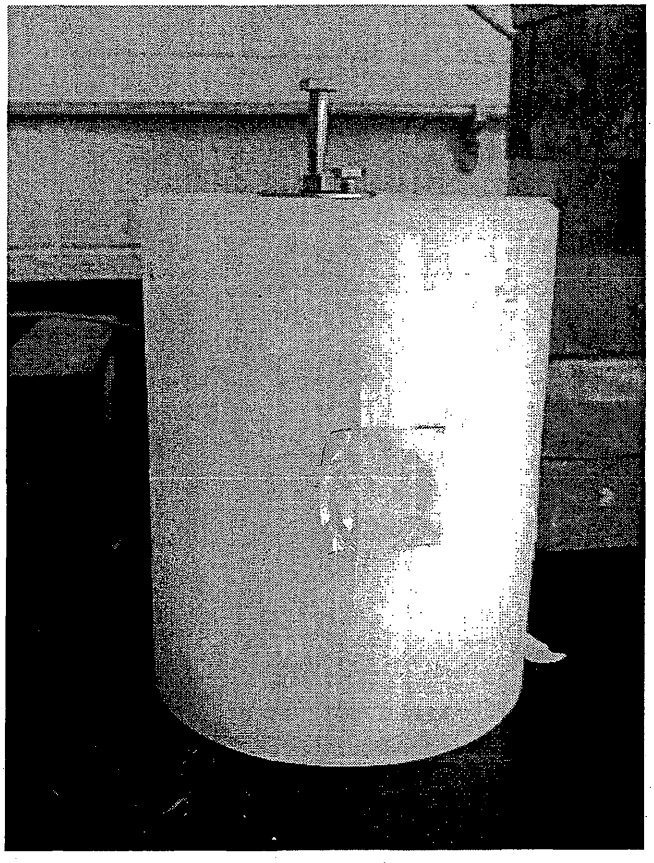

Figure Nineteen: Am/Be radiation source contained in polyethylene cylinder with In foil contained in film sample

For each run, the counts recorded by the Geiger counter as a function of time were extrapolated to determine the number of counts at time = 0 seconds. This was accomplished by graphing ln(A) vs. time, where A represents the number of recorded

counts, the intercept represents the number of counts at time = 0 seconds (Figure Twenty, Equations 1-5 and Figure Twenty-one). For each run, the time was adjusted for the time it took to remove the sample from the neutron source to the time the In foil was placed in the Geiger counter, and the background count was subtracted from the total count. All neutron data can be found in Appendix XIII.

The α_p and β values were also found using the same type of Beer's law analysis that was used in the X-ray absorption testing (see Appendix XII).

$$A = A_0 e^{-(\lambda t)} \qquad \textit{Equation 1}$$

$$t_{1/2} = \ln(2)/\lambda \qquad \textit{Equation 2}$$

$$y=mx+b \qquad \textit{Equation 3}$$

$$\ln(A) = -\left[\ln(2)/t_{1/2}\right]t + A_0 \qquad \textit{Equation 4}$$

$$A_0 = \ln(A) + \left[\ln(2)/t_{1/2}\right]t \qquad \textit{Equation 5}$$

Figure Twenty: Equations relating to In radioactivity

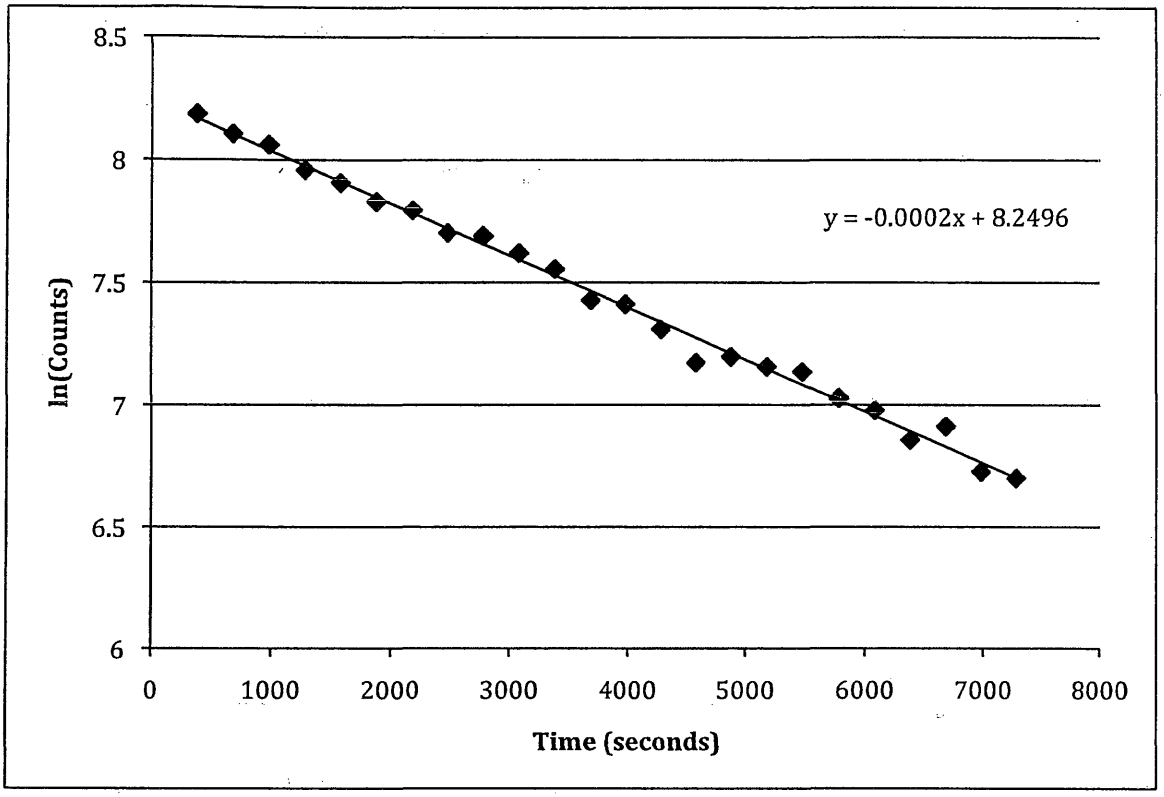

Figure Twenty-one: Graph of ln(recorded counts) versus time for a pure p-HPB/BPF film, where the intercept represents A_0

d. Gadolinium Phenylacetate Characterization

i. Thermogravimetric Analysis

Gadolinium phenylacetate subjected to thermogravimetic analysis using a TA Q500 TGA as previously described. Gadolinium oxide, gadolinium nitrate, and phenylacetic acid were also tested. The TGA graph of gadolinium phenylacetate can be found in Appendix XV.

ii. Elemental Analysis

A sample of gadolinium phenylacetate was sent to Atlantic Microlabs for elemental analysis of percent by weight of C and H.

e. Results and Discussion

i. Polymerizations

Solutions from the most successful polymerizations turned light pink after being heated for about five to ten hours and remained that color until cooled below 150°C.

The amount of potassium carbonate used only seemed to affect the polymerization if under 2.0*x* concentration. Anything over that concentration resulted in no noticeable differences. Under this limit, however, the polymerization apparently did achieve high molecular weight, as the resulting polymer film was brittle and broke when creasing was attempted.

Temperature consistency was the largest obstacle in all of the polymerizations. An oil bath with a magnetic stir bar was used for all polymerizations in order to ensure a uniform temperature throughout the entire round-bottom flask. Furthermore, the entire mixture had to be at least 155°C in order for the reaction to proceed and no higher than 220°C in order to keep the monomer from degrading. If the temperature dropped too much below 155°C, the polymerization slowed and the whole reaction took much longer to complete. A probe regulated hot-stir plate aided in the temperature regulation. One fourth of all polymerizations, however, were still unsuccessful.

ii. Polymer Purifications and Polymer Solutions

Once the polymerization was completed and the toluene was removed from the reaction mixture, a yellow, very viscous solution remained in the round bottom flask. This mixture was slowly poured into a blender containing acetic acid and water. The acetic acid reacted with the potassium carbonate in the mixture to release carbon dioxide with bubbles visible for about five to ten minutes. The content of the blender was then poured into a Büchner funnel and vacuum filtered. The DMAc and potassium and fluoride ions were assumed to wash away with the water. The resulting polymer "fluff" was then washed with boiling deionized water to further remove residual solvent or ions, rinsed with ethanol, and then dried overnight.

Initially, these steps comprised the only purification of the polymer. The polymer was then dissolved in the solvent and pulled into a film. This procedure, however, resulted both in an opaque, dark yellow polymer solution and, correspondingly, an opaque yellow film.

While the opacity of the solution and film was not a problem for instrumental characterization, it presented several difficulties with respect to the addition of the gadolinium salt.

The gadolinium can best function to shield against radiation effectively when it is uniformly dissolved within the polymer. We visibly discerned whether the gadolinium salt was completely dissolved. If the polymer solution and film were not transparent at the start, there was no way to determine if the gadolinium had dissolved in polymer.

For this reason, the polymer purification process was systematically repeated until a clear polymer solution was obtained. Impurities from the polymerization – carbonate,

potassium ions, and residual acetic acid – may have contributed to the opacity. In an effort to improve the purity of the polymer product, the entire process of dissolving the polymer in the solvent, pouring it into the blender, washing, and drying the polymer was repeated several times until a clear polymer solution was obtained.

Additionally, as mentioned in the experimental section, residual acetic acid in the dry polymer from the purification, caused the polymer to turn yellow and harden. To combat this, seven to ten washings with boiling water were added to the filtration process.

Further in the research, it was also observed that one gram of polymer and 5-mL of solvent in small test tubes, tended to leave a white residue floating in the polymer solution. It seemed that this caused the polymer solution to become cloudy. For this reason, the polymer solution was centrifuged prior to making samples.

It also was observed that after heating the polymer solution to 280 $^{\circ}C$, a cloudy solution would became transparent.

The purification process in its entirety was very lengthy. Each time the polymer was added to the solvent, it had to be stirred for one or two full days until all the polymer was dissolved. Then, once the polymer was filtered, it needed to be dried overnight again before it could be used again.

In addition to the increased time, the purification process also greatly decreased the yield of each polymerization. Because of the fluffy nature of the polymer, some material was lost in each transfer from the funnel to a tray for drying, and then again when the polymer was transferred into the Erlenmeyer flasks to be redissolved. Three or more purification cycles led to a considerable loss of polymer. For this reason,

measurements of the mass of the polymer were not taken, as the continued transfer of the polymer into a container to measure its mass would have resulted in an even greater loss of polymer.

iii. Gadolinium Salt Synthesis

Regulation of the pH was the most important factor in the gadolinium salt synthesis. Below a pH of 5, the phenylacetic acid did not dissolve in water. If too much ammonium hydroxide was added and the pH rose above six, precipitation still occurred, however, the solid was insoluble in both NMP and DMAc. TGA data for this precipitate did not exhibit more than a 5% mass loss and the resulting TGA graph was almost identical to the graph of gadolinium oxide. Overshooting the pH range, however, was easily remedied by adding nitric acid dropwise into the phenyacetic acid/ammonium hydroxide mixture until the pH returned to the 5-6 range.

Although the procedure for the synthesis of gadolinium salt was reported in the literature, there is no reported characterization of the salt [22]. TGA analysis was consistent with what would be expected for gadolinium phenylacetate, given molar values and remaining weight percent and assuming that gadolinium phenylacetate will decompose to gadolinium oxide. By determining that 66% of the original mass was lost and using the molecular weights of both gadolinium phenylacetate and gadolinium oxide, it was found that there should have been 1.95 milligrams of gadolinium oxide remaining, compared to the 2.06 milligrams that were actually remaining. Given that the mass of the

sample measured in the TGA can fluctuate, this fits with a margin of error that the salt we produced could be gadolinium phenylacetate.

The TGA graph of gadolinium phenylacetate is attached as Appendix XV. TGA was also run on phenylacetic acid and gadolinium nitrate and was compared to the synthesized gadolinium phenylacetate to definitively rule out the possibility that the precipitate was either of the starting products.

Elemental analysis for carbon and hydrogen by Atlantic Microlab, Inc. supported the conclusion that that salt precipitated was, indeed, gadolinium phenylacetate.

The results of the analysis are given in Table X. The theoretical and measured weight percents of carbon and hydrogen are close. It is concluded, therefore, that the salt synthesized is gadolinium phenylacetate.

Element	**Theoretical wt.%**	**Experimental wt. %**	
C	51.23	50.14	50.24
H	3.76	3.81	3.67

Table X: Results of elemental testing by Microlab, Inc.

Gadolinium phenylacetate melted at 175-176°C. No reports of the melting temperature were found in the literature, so no comparison is possible.

iv. Film Preparation

Films were prepared by pouring the polymer solution onto a plate of glass and then dragging a drawing blade over the solution in order to achieve a thin film. A steady

hand when pulling the drawing blade and drying the glass plates with a hot air gun usually yielded good films.

Problems that did arise with the film preparation were often due to glass that was not completely clean. In such instances, after the film was pulled, small holes appeared on the film where the polymer solution had pulled together leaving small circles of exposed glass.

Furthermore, if the dry box was left open for too long after the film was pulled, the polymer film would be exposed to water vapor in the air and begin to turn opaque.

Both the tack free box and the oven had to be leveled before each use or the polymer film would run, causing the film to be uneven in its thickness.

Problems also arose with the curing environment of the thick film samples. While TGA results with the sample in a nitrogen atmosphere showed that gadolinium phenylacetate degraded around 320°C, the films were not cured in a nitrogen environment; the early degradation of the organic part of the salt could have been caused by oxidation.

For this reason, an oven was set up through which nitrogen was passed thereby eliminating air in order to prevent the bubbling that only seemed to be a major problem with the films that contained gadolinium.

In another trial, the polymer solution was heated to 280°C before the sample was poured. Initially, the samples were completely clear. Once they were placed in the oven at 85 °C, however, the films seemed to grow an opaque film on top. This may have been the organic decomposition product.

v. Thick Sample Preparation

All of the methods attempted are outlined in Appendix VIII and are described in the procedure section.

With slow and long enough curing procedures, it was possible to make pure, thick films in oxygen (See Appendix VIII, Film ID: T-MP-HPB-04, T-MP-HPB-05, T-P-HPB-01, VT-MP-HPB-01). Samples that contained gadolinium phenylacetate, however, bubbled when cured in air.

This observation led to the assumption that the organic part of the gadolinium salt must be decomposing during the curing process, causing the bubbling of the thick samples.

An attempt was made, therefore, to decompose the organic part of the salt prior to the curing procedures. The sample solutions were heated up to 300 ° on a heater/stir plate and left to mix for over a day before the samples were poured and cured. This, however, had no effect on the final condition of the sample.

A vacuum oven was modified so that nitrogen, instead air was present in the oven while the samples were curing. This seemed to solve the bubbling problem, as many samples containing gadolinium phenylacetate were made in this way without bubbles.

The use of nitrogen while curing the samples, however, did not yield a good sample in all cases. It seemed that, although the samples were not bubbling, a phase separation was occurring within the sample. The top layers of many samples were coated in a white, uneven layer that was only present on the very top of the sample. In some cases, this top layer seemed to have caused the samples to crack or have very uneven thicknesses. It was proposed that the NMP was coming off the sample too quickly;

causing any impurities or the decomposed organic part of the salt to separate from the polymer.

In order to stop this from occurring, a large Petri dish was placed on top of a 5 wt-% Gd sample. The dish was propped open with a few pieces of scrap metal. The idea was that this would allow the NMP vapor to collect over the sample, so that the pressure of the NMP in the sample and above the sample was similar. It was anticipated that this might prevent the phase separation from occurring. The sample was held at 60°C for three days, and then the temperature was raised approximately 10°C a day until reaching the final temperature of 230°C. The resulting sample did not exhibit any phase separation and contained only one small bubble.

vi. Polymer Characterization- Viscosity

The viscosity was measured in order to ensure that high molecular weight polymers had been synthesized. Only clear solutions were tested. Cloudiness in a solution suggests that there are undissolved particles that would affect the viscosity test by causing drag and holes in the solution. Such conditions would not allow for a constant viscosity to be measured.

All viscosity data obtained are in Appendix IX. For all of the measurements, the viscosity remains almost independent of the shear rates used. All of the solutions, therefore, were Newtonian in nature. Table XI summarizes the results.

Solution ID	% Gd	Average Viscosity (cP)	Tg (°C)
L-P-HPB-01, Batch 1	0	7400	159
L-P-HPB-02, Batch 2	5	6920	159
L-P-HPB-03, Batch 1	10	7440	160
L-P-HPB-04, Batch 2	15	6910	161
P-HPB- Incomplete Polymerization	0	370	None

Table XI: Average viscosities of p-HPB/BPF solutions

L-P-HPB-01 and L-P-HPB-03 were made from the same polymer batch; L-P-HPB-02 and L-P-HPB-04 were made from the same polymer batch. Correspondingly, each polymer batch has similar viscosity. The increase of gadolinium concentration does not seem to have an effect on the viscosity; the source of the batch seems to be the only factor which is affecting the viscosity. Films made from solutions L-P-HPB-01 through L-P-HPB-04 had thermal data comparable to the literature values of similar polymers [17]. The film made from the incomplete polymerization did not even have a noticeable glass transition temperature (Section IV, c, iv).

There are no other existing viscosity data with which to compare these results, so the viscosity data obtained are only relative. Furthermore, previous research concluded that if a polymer film is not brittle and is able to be creased, the polymer has reached a high molecular weight during the polymerization [11]. In general, it seems reasonable to conclude that, if the glass transition temperatures of a given film are comparable to the literature values and the films are also creaseable, the films have obtained a high enough molecular weight for this research.

vii. Polymer Characterization- Thermogravimetric Analyses

Thermogravimetric analyses were conducted in order to determine the temperatures which the polymers could withstand before they began to degrade and to determine if the addition of gadolinium had any effect on the thermal stability of the polymer.

Generally speaking, all test results were very good. All of the results can be found in Appendix VII and VIII and a summary of the average TGA data for all polymer films can be found in Table XII.

Polymer Type	Average 10% Degradation Temperature (°C)
BPA/BPF	504
p-HPB/BPF	501
m-HPB/BPF	502
m-HPB/p-HPB/BPF	503

Table XII: Average TGA data for each polymer type

TGA analysis showed that all the polymers displayed high thermal stability, as shown by the high temperatures for 5% and 10% degradation (see Appendix VII). All samples tested were stable above 400°C, and many polymer films showed no mass loss until almost 500°C. Furthermore, TGA results show that the solvent has been removed from the films prior to testing, as there were no polymer films that showed mass loss around the boiling point of the solvent NMP (202°C). Some thick samples, however, did show a slight mass loss around 200°C, therefore, not all of the NMP was evaporated in the oven.

In some instances, when the films contained a high gadolinium concentration, the 5% degradation temperature was lower than for the rest of the samples, however the 10% degradation temperature was fairly consistent.

viii. Polymer Characterization- Differential Scanning Calorimetery

Differential scanning calorimetery measurements were conducted to ensure that the polymerizations had produced the desired polymer and that there was some consistency among the same polymers. Generally speaking, all test results were very good. All of the results can be found in Appendix VII and a summary of the average DSC for all polymer films can be found in Table XIII. In one case, a *p*-HPB/BPF polymerization was stopped before it could be completed and a film was pulled for testing. No glass transition temperature was found for this film.

Polymer Type	Average Glass Transition Temperature (°C)
BPA/BPF	154
p-HPB/BPF	160
m-HPB/BPF	124
m-HPB/p-HPB/BPF	140

Table XIII: Average glass transition temperature for each polymer type

No crystalline melting temperature was observed below 300°C. Furthermore, the differences in glass transition temperatures of the polymer films having different molecular structures can be explained. As mentioned with the polyimides, polymers with rigid, extended molecular structures have higher glass transition temperatures, as they are

less able to move and rotate internally. This is consistent with the DSC results. Polymer films made with *p*-HBB, an elongated, rigid monomer due to para substitution, have glass transition temperatures around 160°C. Polymers made with *m*-HPB, a monomer with more flexibility due to meta-substitution, which introduces a new kink into the polymer chain, exhibited lower glass transition temperatures around 120°C. Polymers made with BPA, a monomer with a structure similar to *p*-HBP, only smaller, exhibited glass transition temperatures slightly lower than that of *p*-HBP, around 150°C. When polymers were made of both *p*-HPB and m-HPB, the resulting glass transition temperatures, 140°C, were measured to be in between the glass transition temperatures of those polymers made with only one bisphenol species. Thus, the copolymer has "average" properties of the two homopolymers.

Pure films were also made by combining 1:1 mass ratios of each of the HPB polymers in solution (*m*-HPB/BPF was dissolved with *p*-HPB/BPF, *m*-HPB/BPF was dissolved with *m*-HPB/*p*-HPB/BPF, etc). For naming purposes, a mixture of *p*-HPB/BPF with *m*-HPB/BPF was called MIX-P-M-HPB.

The DSC data show that in each case the glass transition temperature is intermediate between the two polymer's individual *T*g's (See Table XIV). For MIX-P-M-HPB, the glass transition temperature is half way between the glass transition temperatures of m-HPB/BPF and p-HPB/BPF. For MIX-MP-P-HPB, the polymer is three-quarters *p*-HPB/BPF and its glass transition temperature is about three-quarters the way between the glass transition temperatures of *m*-HPB/BPF and *p*-HPB/BPF. MIX-MP-M-HPB demonstrates this same pattern (See Figure Twenty-two). This seems to

indicate that all of the polymer combinations are compatible, and thus do not experience phase separation.

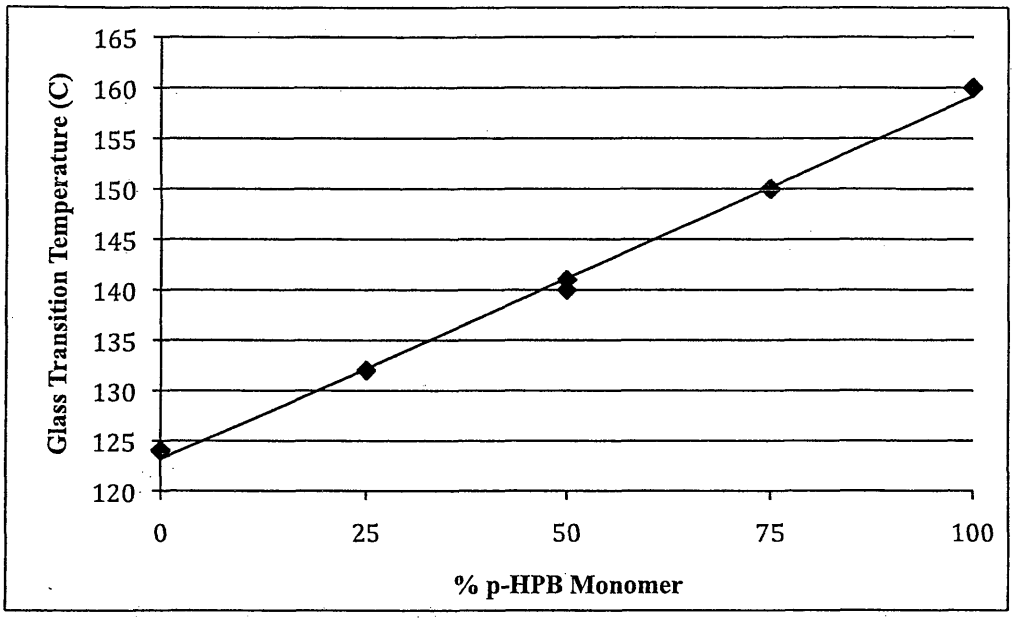

Figure Twenty-two: Graph of glass transition temperature vs. % p-HPB monomer

That is, if two distinct Tg's had been observed for a polymer mixture, it would have meant that the two polymers were not miscible and not compatible. However, Hourston and Song have conducted research into polymer blends and miscibility, and they have concluded that the DSC is not capable of distinguishing two separate Tg's if the difference of the Tg's between two polymers in a blend is less than 15 °C [18]. In this study, the only mix in which the individual polymers had Tg differences of greater than 15°C (MIX-P-M-HPB), had only one visible Tg. It can be concluded, that those two polymers *m*-HPB/BPF and *p*-HPB/BPF are indeed compatible. It seems, therefore, reasonable to also conclude that the other two polymer blends, which are more similar than *m*-HPB/BPF and p-HPB/BPF are also compatible.

Furthermore, these data indicate that the glass transition temperatures can be adjusted by preparing pure copolymers with different m-HPB /p-HPB ratios or by mixing pure polymers to achieve desired ratios.

Film	Glass Transition Temperature (°C)
MIX-P-M-HPB	141
MIX-MP-P-HPB	150
MIX-MP-M-HPB	132
m-HPB/BPF	124
p-HPB/BPF	160
m-HPB/p-HPB/BPF	140

Table XIV: Glass transitions of HPB polymers and HPB polymer mixtures

The measured glass transition temperature (154°C) of the BPA/BPF polymer is also consistent with other data obtained in this laboratory. Hue et al. has found the glass transition temperatures of the same polymer (Appendix VII, reference numbers BF-01 through BF-05) to be a little higher at 162°C [11]. The difference may be explained by the inevitable differences in the polymerization reaction and work-up.

ix. Polymer Characterization- Tensile Testing

The tensile testing was conducted in order to measure the strength of the films fabricated in this research and to determine if the incorporation of gadolinium into the films had an appreciable adverse effect on the films' strength.

Poly(arylene ethers), in general, have already been demonstrated to be quite strong, hence their use as engineering polymers [27]. It was previously unknown,

however, whether the addition of gadolinium would have an adverse effect on the tensile strength of the films.

Ideally, a load of 50 N would have been used in order to achieve more precise measurements, given that most of the films broke with a maximum load less than 50 N. The 50 N load, however, was malfunctioning and the only other available load was 2500 N.

Furthermore, in the initial tests, the film strip slipped out of the clamp prior to the breaking point. Even after tightening the clamps with a ratchet, the films pulled out of the top of the clamp before the test was completed. For this reason, one side of each clamp was roughed with horizontal lines, and the other was roughed with "x's" so that the clamp might hold the film more tightly (See Figure Twenty-three).

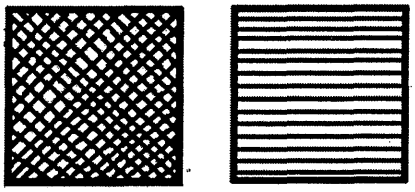

Figure Twenty-three: Diagram of how insides of the clamp were roughed

While the roughening did eliminate the slippage, this solution caused more problems. Many of the films tested broke inside the clamps. After the films were removed from the clamps, it became apparent that the roughening on the inside of the clamps was creating weak points in the film. Thus, the film was breaking under the load at these points within the clamps. The data from the films that broke inside of the clamps were, therefore, excluded.

Another problem with the tensile testing was that many of the films had imperfections, which also created points of weakness. Imperfections were consequences of creases in the film, uneven strip thicknesses, and uneven film width. In some cases, small particles of polymer which must not have completely dissolved in the solvent prior to curing were also visible and produced weak points in the film.

It was found that pure films had maximum loads up to 45N and elastic moduli up to 172000 N/m. Films that contained gadolinium had maximum loads up to 54 N and elastic moduli up to 244000 N/m. It does not seem, therefore, that the addition of gadolinium weakens the film strength. Appendix X contains all tensile data.

Commercially produced Kapton, an aromatic polyimide (see Figure Twenty-four) available from DuPont, was also tested using the same instrument. The six strips tested had an average maximum load of 45 and an elastic modulus of 94000 N/m. Kapton is widely used for automotive, aerospace, and electrical applications. Its versatility is due to its high thermal stability and strength. Given the similarity to the maximum loads for both Kapton and the synthesized films, the poly(arylene ether) films showed comparable strength. Furthermore, the Kapton strips tested had an average elastic modulus lower than any of the poly(arylene ether) films tested.

Tensile testing data can be found in Appendix X.

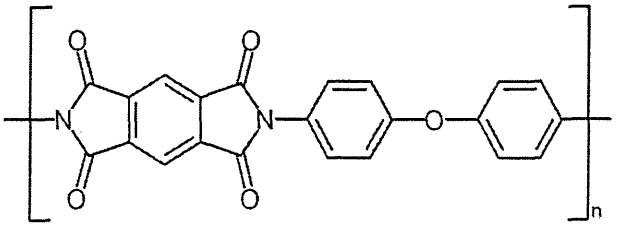

Figure Twenty-four: Structure of Kapton

x. Polymer Characterization- X-Ray Absorption Testing

X-ray absorption testing shows that poly(arylene ethers) will effectively shield against X-rays. Appendix XI contains the X-ray data for all of poly(arylene ether) films tested, including film thicknesses and the percentage of the incident X-rays that the films has shielded. Pure films shield only 2-3% of the X-rays, however, 15 wt-% gadolinium-containing films shielded up to 27% of the X-rays. Gadolinium, therefore, has been shown to be an effective additive to shield against high energy EM radiation. Appendix XII contains the graphs of the Beer's law analysis for each of the polymer types.

The data also show consistency in the effective contribution of gadolinium to the overall shielding capabilities of the polymer, represented by β. (See Figure Nine, Equation Three). While the contribution of the polymer to the shielding abilities of the film, α_p, varies for each polymer type, β remains relatively consistent, as would be expected as the gadolinium additive is the same in each polymer type (see Table XV). Figure Twenty-five is an example of a Beer's law plot with the least-squares line and equation, where the negative slope represents β and the negative intercept represents α_p.

Polymer Type	β **(mm^{-1})**	α_p **(mm^{-1})**
p-HPB/BPF)	27	22
m-HPB/BPF	27	36
m-HPB/p-HPB/BPF	23	46
BPA/BPF	28	32

Table XV: X-ray absorption α_p and β values for poly(arylene ethers)

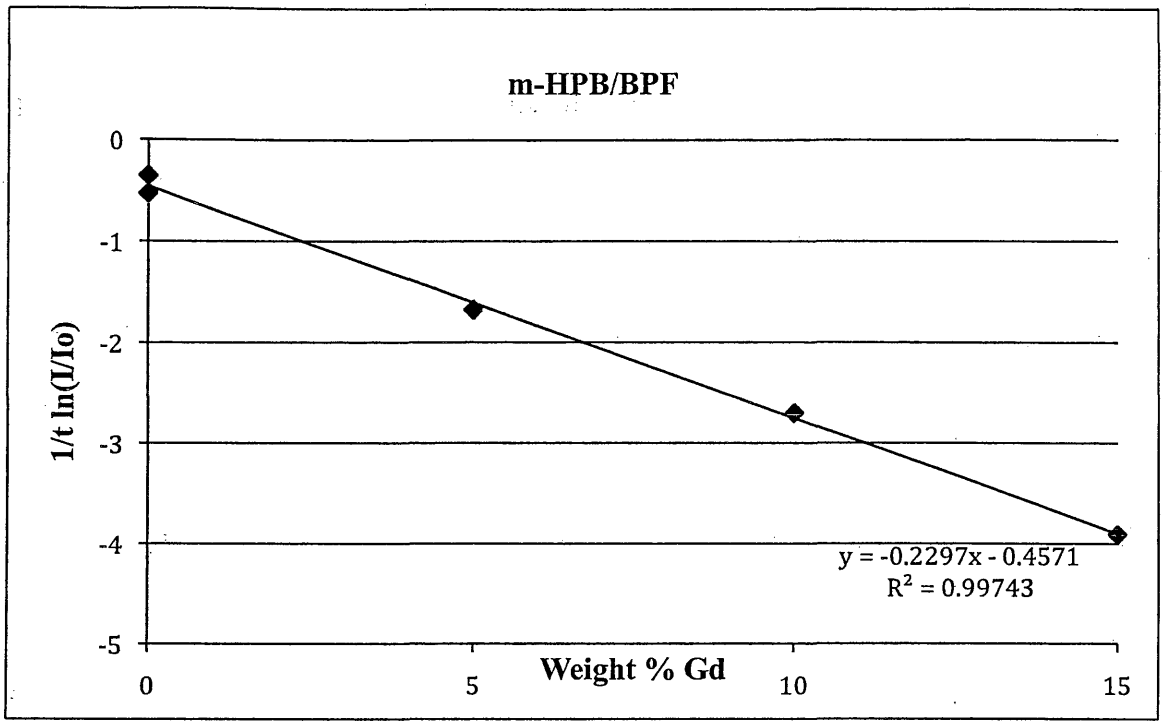

Figure Twenty-five: Beer's Law analysis for X-ray absorption for m-HPB/BPF

Furthermore, thick samples are able to absorb 99-100% of the incident X-rays (see Table XVI). Because most all of thick films bubbled, however, the thicknesses are only approximate.

Polymer ID	%Gd	Approximate Thickness (mm)	% X-Rays Absorbed
T-P-HPB-01	0	1.0	25
S-MP-HPB-01	0	1.7	66
VT-MP-HPB-02	5	2.1	82
VT-MP-HPB-03	10	1.6	100
VT-MP-HPB-04	15	1.5	99
VT-M-HPB-01	0	2.0	76
AG-M-HPB-03	10	1.4	97
AG-M-HPB-04	15	1.8	100

Table XVI: X-ray absorption data for poly(arylene ether) thick films

Given the α and β values that were found from each polymer type, a graph can be made that plots the percentage of X-rays absorbed by the sample by the weight percent gadolinium for a hypothetical film with a thickness of one millimeter (see Equations One and Two, Figure Nine). Films with 15 wt.-% Gd are estimated to absorb up 99% of incoming X-rays (See Figure Twenty-six).

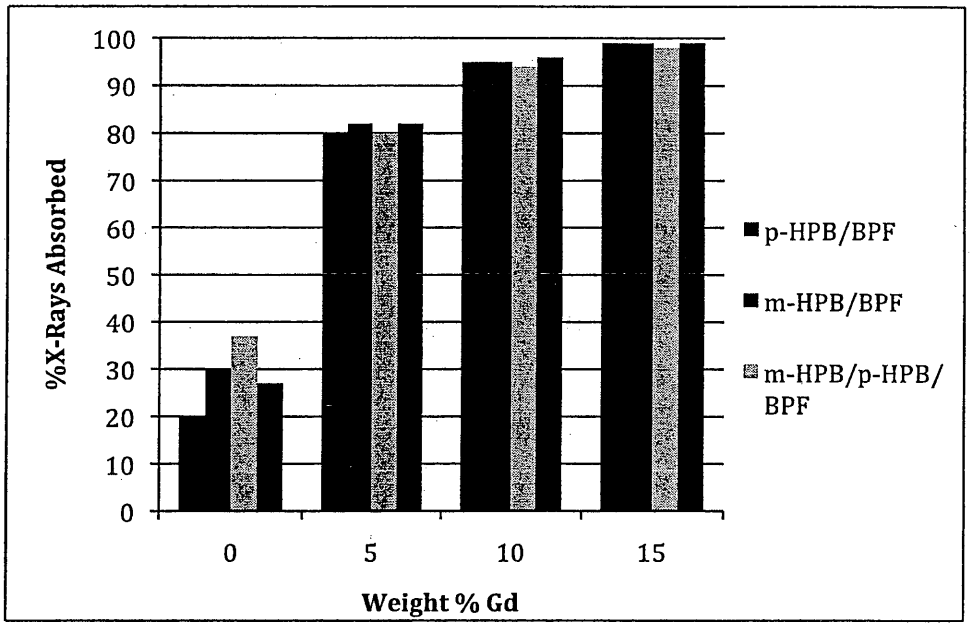

Figure Twenty-six: Graph of the percentage of X-rays absorbed vs. wt-% Gd for each of the poly(arylene ethers) synthesized in this research, for a hypothetical 1.00mm thick sample

xi. Neutron Absorption Testing

Neutron absorption testing showed that, for the most part, poly(arylene ether) films containing gadolinium absorbed neutrons. Appendix XIII contains all of the data for the films tested, including wt-% Gd, film thickness, extrapolated A_0 values, and the

percentage of neutrons absorbed. Pure films shielded almost none of the neutrons, however, a 10 wt-% gadolinium-containing film with a thickness of only 0.06mm shielded up to 10% of the neutrons. Gadolinium, therefore, appears to be an effective additive to shield against neutrons. Appendix XIV contains the graphs of the Beer's law analysis for each of the polymer types. Table XVII contains the α_p and β values for each polymer type (See Figure Nine, Equation Three).

Polymer Type	α_p **(mm^{-1})**	β **(mm^{-1})**
p-HPB/BPF	23	15
m-HPB/BPF	2	12
m-HPB/p-HPB/BPF	7	12

Table XVII: Neutron absorption α_p and β values of each polymer type

The data also show consistency in the effective contribution of gadolinium to the overall shielding capabilities of the polymer, represented by β. While the contribution of the polymer to the shielding abilities of the film, α_p, varies for each polymer type, β remains relatively consistent, as would be expected.

The 15 wt-% Gd samples, however, were left off in the Beer's law analysis because for both the *m*-HPB/*p*-HPB/BPF and *p*-HPB/BPF polymers, the number of extrapolated number of counts were irregularly high. It is not known with certainty what causes this abnormality within the data; however, other research in this lab has found the same phenomenon with other metal additives at 15 wt-% concentrations [17].

One explanation may be that, in the 15wt-% films, the gadolinium was not evenly distributed throughout the film, which caused an effective decrease in the number of gadolinium particles with which the neutrons could interact. While it seems that the gadolinium is uniformly distributed throughout the polymer in solution, this agglomeration of the gadolinium may occur while the film is being cured in the oven. There may be some limit to the amount of gadolinium phenylacetate that can be added to a film before the agglomeration occurs. This research indicates that the limit may be between 10 and 15 wt-% Gd.

X. Conclusions

For longer-term exploration to even be practical, improved radiation shielding materials must be developed to protect humans and their equipment. In this regard, a U.S. National Academies' report has recognized that radiation protection research should be expanded and more adequately funded.

In this research, various polyimides and poly(arylene ethers) were synthesized to obtain a high hydrogen content for increased shielding capabilities against galactic cosmic radiation and to obtain a molecular structure for increased structural stability. Modified tungsten was added to polyimides and gadolinium compounds were incorporated into the poly(arylene ethers) in order to add protection against short wavelength electromagnetic radiation, and in the case of gadolinium, neutrons. Clear poly(arylene ether) solutions were developed to ensure that the gadolinium compounds incorporated within the polymer were distributed evenly at a molecular level.

All of the polymers synthesized have high glass transition temperatures, indicating their suitability for use in outer space. The incorporation of the tungsten or gadolinium compounds did not appear to affect any of the glass-transition temperatures.

Furthermore, the glass transition temperatures of the different poly(arylene ether) films can be rationalized in terms of their molecular structure. Rigid polymers have higher glass transition temperatures, as they are less able to move and rotate internally. This is consistent with the DSC results. Polymers made with *p*-HPB, a relatively rigid monomer due to para substitution, have glass transition temperatures around 160°C. Polymers made with *m*-HPB, a monomer with more flexibility due to meta substitution which introduces a kink into the polymer chain, have lower glass transition temperatures

around 120°C. Polymers made with BPA, a monomer with a structure similar to *p*-HBP, only smaller, exhibited glass-transition temperatures slightly lower than that of *p*-HBP, around 150°C. When polymer films were made of both *p*-HPB and *m*-HPB, or made of two polymers containing varying ratios of the two monomers, the resulting glass-transition temperatures were in between the glass-transition temperatures of those polymers made with only one bisphenol species. The copolymer has "average" properties of the two homopolymers. Thus, the glass transition temperature can be adjusted by synthesizing either a polymer with the correct ratio of m-HPB to p-HPB or by mixing pure polymers to attain the preferred ratio.

TGA results show that all of the polymer films synthesized in this research are thermally stable at high temperatures and that neither the modified tungsten or the gadolinium phenylacetate had much impact on the thermal properties of the film. This research thus revealed that the synthesized polymers are promising candidates for application in extremes of outer space.

While it had already been demonstrated that poly(arylene ethers) are strong, tensile testing confirms that the polymers synthesized in this laboratory have similar maximum loads and elastic moduli to Kapton, a widely used, commercially available polymer.

This study showed that the tungsten additive did not contribute greatly to the shielding of X-ays by the polyimides. All films, whether they contained the additive or not, absorbed around 10% of the incident X-ays.

X-ay absorption testing with poly(arylene ethers), however, revealed that the addition of gadolinium compounds greatly enhanced the x-ray shielding capabilities of

the polymer. A Beer's law analysis of the films for each polymer type allows the contribution of radiation absorption properties of the polymer and the gadolinium (α_p and β) to be quantified. Furthermore, a 10 wt-% thick sample of only an approximate thickness of 1.6 mm was shown to absorb 100% of the incident X-rays. Given the α_p and β values of the various polymer types, it can predicted that a 15 wt-% sample with a thickness of only 1.0 mm should absorb almost 100% of the incident X-rays.

Neutron absorption testing with poly(arylene ethers) also revealed that the addition of gadolinium compounds up to 10 wt-% Gd greatly enhanced the neutron shielding capabilities of the polymer. As with the X-ray testing, α_p and β can be quantified.

The methodology and characterization used in this research has furthered an understanding of radiation protection technology, and new materials have been created that can be utilized in outer space.

References

[1] "Program: Mars Exploration." National Aeronautics and Space Administration, United States of America White House. <http://www.whitehouse.gov/omb/budget/fy2004/pma/marsexploration.pdf>.

[2] Committee On The Evaluation Of Radiation Shielding For Space Exploration, National Research Council. "Managing Space Radiation Risk in the New Era of Space Exploration." Washington, D.C.: National Academies Press, 2008.

[3] Aeronautics Research Mission Directorate, *X6.01 Radiation Shielding Materials.*

[4] Rapp, Donald. "Radiation Effects and Shielding Requirements in Human Missions to the Moon and Mars." *The International Journal of Mars Science and Exploration* (2006) 46-71.

[5] Wilson, J; Shinn J.; Tripathi,R; Singleterry,R; Clowdsley,M; Thibeault,S; Cheatwood,F; Schimmerling,W; Cucinotta, F; Badhwar,G; Noor,A; Kim,M; Badavi,F; Heinbockel,J; Miller,J; Zeitlin,C; Heilbronn,L. "Issues in deep space radiation protection." *Acta Astronautica* 49 (2001): 289-312.

[6] Simpson, J. A.; "Elemental and Isotopic Composition of the Galactic Cosmic Rays," *Annual Reviews of Nuclear and Particle Science* 33 (1983): 323-381.

[7] Churchill, R; Aquino, E; Orwoll, R; Kiefer R; "Multifunctional Polymers Incorporating High-Z Neutron-Capture Nanoparticles," NASA Phase I Final Report.

[8] Ehman, William D., and Diane E. Vance. *Radiochemistry and Nuclear Methods of Analysis*. Vol. 116. New York: John Wiley & Sons, Inc., 1991.

[9] Cotter, Robert. *Engineering Plastics*. Durham, NH: Gorden and Breach, 1995.

[10] Hue, Lucy; Miller Adriane; Park, Chang; Plichta Kristen; Rochford, S; Schultz M; Yang, S; Orwoll, R. "Aliphatic/Aromatic Hybrid Polymers for Functionally Graded Radiation Shielding." *High Performance Polymers* 18 (2006): 213-225.

[11] Harbert, Emily; "Poly(arylene ether) Synthesis and Incorporation of Gadolinium Compounds for Improvement of Radiation Shielding for Use in Outer Space," Senior Thesis, College of William and Mary, Williamsburg, Va. 2004.

[12] Rabilloud, Guy. *High-Performance Polymers: Chemistry & Applications 2 Polyquinoxalines and Polyimides*. Minneapolis: Editions Technip, 1999.

[13] Leu, Tsu-Sang, and Chan-Shan Wang. "Synthesis and Properties of Polyimides Containing Bisphenol Unit and Flexible Ether Linkages." *Journal of Applied Polymer Science* 87.6 (2002): 945-52.

[14] Harris, Frank. "Synthesis of Aromatic Polyimides From Dianhydrides and Diamines." *Polyimides* (1990): 1-37.

[15] Rodgers, Martin; Timothy Long, eds. *Synthetic Methods in Step-Growth Polymers*. Hoboken, NJ: Wiley-Interscience, 2003.

[16] Churchill, R; Aquino, E; Orwoll, R; Kiefer R; "Hydrogen-rich, Multifunctional Polymeric Nanocomposites for Radiation Shileding," NASA Phase I Final Report

[17] Private Conversation with Robert Orwoll, Ph.D., College of William and Mary.

[18] Hourston, Douglas J., and Mo Song. "Applications of Modulated Temperature Differential Scanning Calorimetry to Polymer Blends and Related Systems." *Modulated Temperature Differential Scanning Calorimetry Theoretical and Practical Applications in Polymer Characterization* (2008): 161-215.

[19] Hergenrother, P; Jensen B; Havens S. "Poly(arylene ethers)." *Polymer* 29 (1988): 358-369.

[20] Hergenrother, Paul M. "Recent developments in poly(arylene ether)s containing heterocyclic units." *Macromolecular Reports* A31.Suppl. (1994): 731-38.

[21] Hergenrother, Paul M. "New Developments in Thermally Stable Polymers." *Journal of the Royal Netherlands Chemical Society* 110.12 (1991): 481-491.

[22] Keli, Z; Jibing, Y; Liangjie, Y; Jutang S. "Synthesis and Thermal Decomposition Mechanism of Rare Earth Benzoates." *Journal of Rare Earth Benzoates* 17.4 (1999).

[23] Brookfield engineering Lab., Inc. *More Solutions to Sticky Problems: A Guide to Getting More From Your Brookfield Viscometer*. Brookfield engineering Lab., Inc.

[24] Private Conversation with Richard Kiefer, Ph.D., College of William and Mary.

Appendix I: Thin Film Rating System

1	perfect- no bubbles or specks , creaseable
2a	above average-no bubbles, few specks, creaseable
2b	above average-no bubbles, slightly uneven polymer distribution, creaseable
2c	above average-no bubbles, few specks and slightly uneven polymer distribution, creaseable
3a	average- many specks, creaseable
3b	average- moderately uneven polymer distribution, creaseable
3c	average- many specks, moderately uneven polymer distribution, creaseable
4a	below average- bubbles, creaseable
4b	below average- bubbles, very uneven polymer distribution, creaseable
5	failure- not creaseable

Appendix II: Index of all polyimide films including rating, TGA, and DSC data

Film ID	Monomers	% Polymer	%W	Creaseable	Rating	5% Degradation (°C)	10% Degradation (°C)	Tg (°C)
BAMBT-01	BAM/BTDA	15	0	yes	1	500	512	211
BAMBT-02	BAM/BTDA	20	0	yes	3b	509	530	210
BAMBT-03	BAM/BTDA	20	5	yes	3b	481	492	223
BAMBT-04	BAM/BTDA	20	10	no	5	488	498	223
BAMBT-05	BAM/BTDA	20	15	yes	2b	483	492	219
BAMBT-06	BAM/BTDA	17	0	yes	2b	495	508	217
ODABT-01	ODA/BTDA	15	0	yes	3b	518	544	268
ODABT-02	ODA/BTDA	15	0	yes	3b	522	546	285
ODABT-03	ODA/BTDA	15	0	yes	2b	501	541	276
ODABT-04	ODA/BTDA	15	0	yes	3b	514	534	273
ODABT-05	ODA/BTDA	15	0	yes	3b	513	540	273
ODABT-06	ODA/BTDA	20	0	yes	2b	522	538	279
ODABT-07	ODA/BTDA	20	5	yes	3b	524	548	275
ODABT-08	ODA/BTDA	20	10	yes	3b	525	543	277
ODABT-09	ODA/BTDA	20	15	yes	3b	536	551	279
ODABT-10	ODA/BTDA	17	5	yes	2b	528	546	276
ODABT-11	ODA/BTDA	17	10	yes	2b	544	567	274
ODABT-12	ODA/BTDA	17	15	yes	1	542	564	279
ODABT-13	ODA/BTDA	17	n/a	yes	4b	534	546	277

Appendix III: Example TGA graph

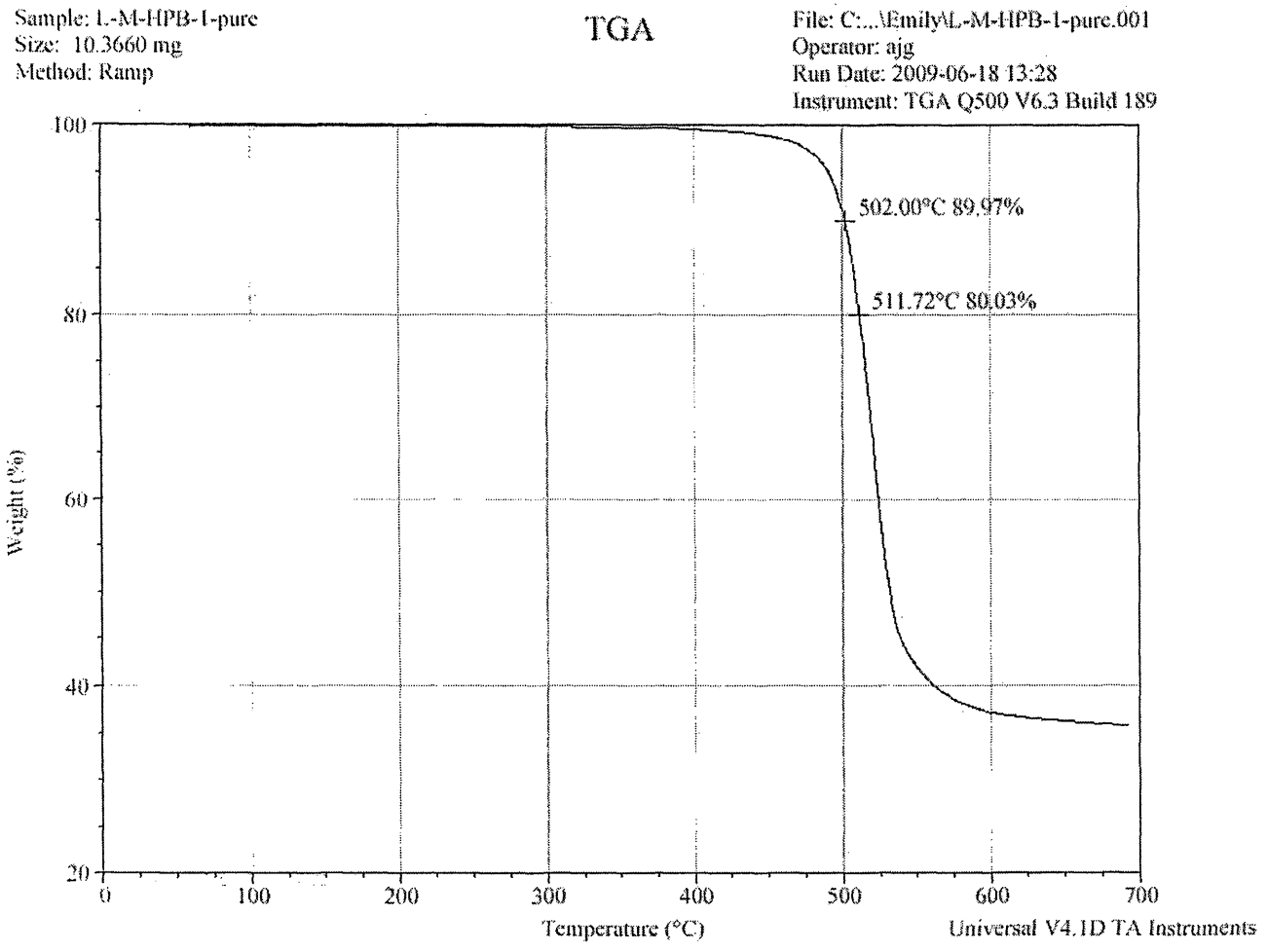

Appendix IV: Example DSC graph

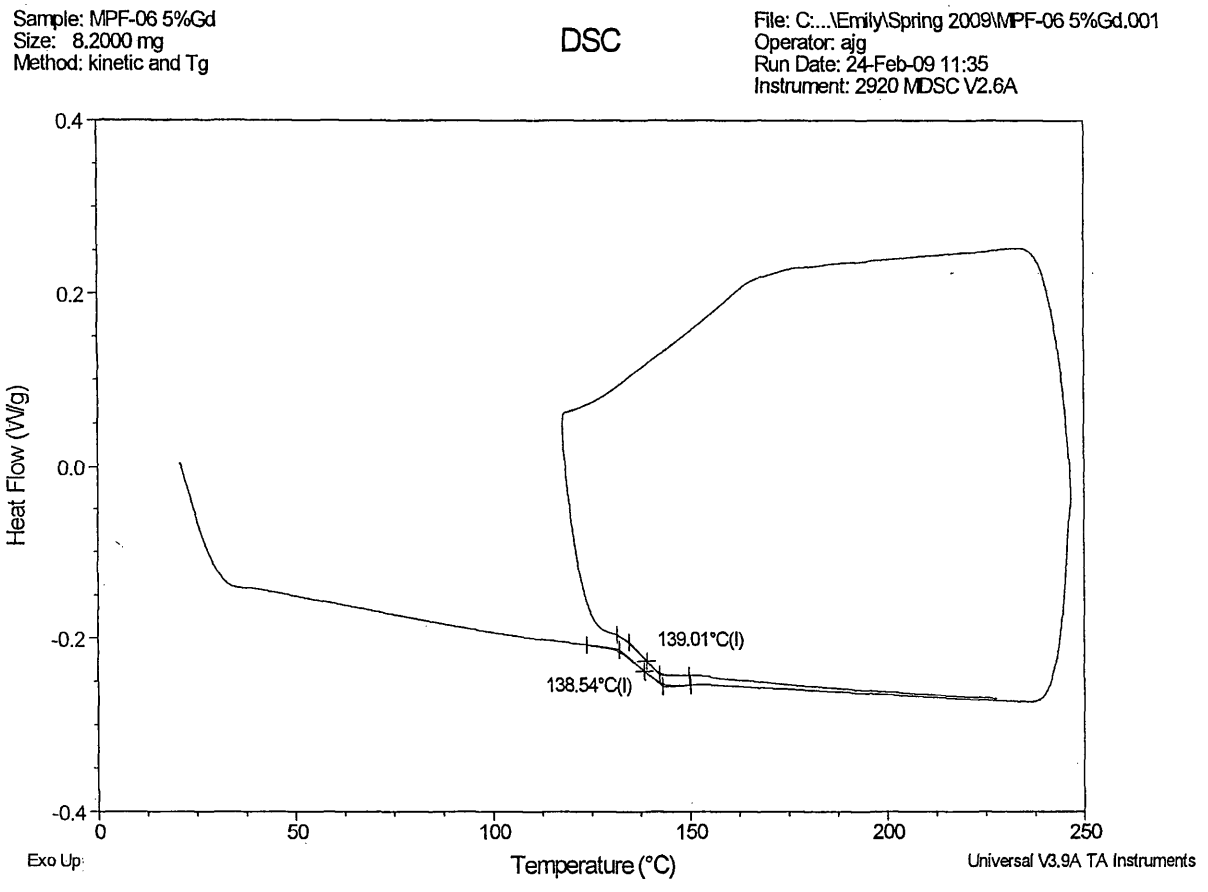

Appendix V: Polyimide x-ray absorption Beer's law analysis graphs

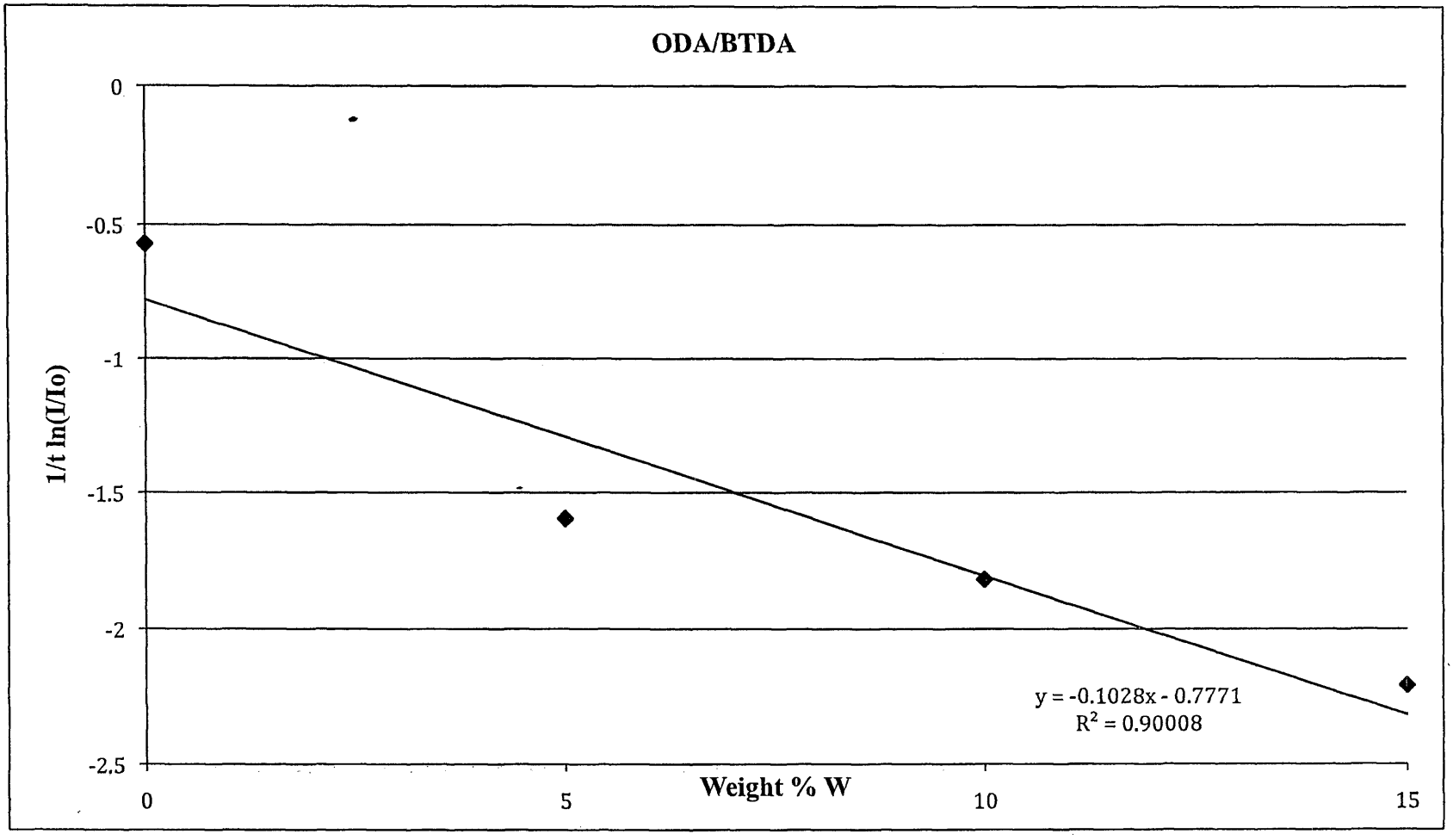

Appendix VI: Polyimide X-ray data

Film ID	% W	3x3 Thickness (mm)	% X-Rays Absorbed
BAMBT-01	0	0.013	1.3
BAMBT-03	5	n/a	n/a
BAMBT-04	10	n/a	n/a
BAMBT-05	15	0.024	10.2
BAMBT-06	0	0.030	1.6
ODABT-01	0	n/a	n/a
ODABT-04	0		2.4
ODABT-06	5	0.055	8.4
ODABT-08	10	n/a	n/a
ODABT-09	15	n/a	n/a
ODABT-10	5	0.059	10.1
ODABT-11	10	0.045	9.5
ODABT-12	15	0.048	10

Appendix VII: Index of all poly(arylene ether) films including rating, TGA, and DSC data

Film ID	Monomers	% Gd	Creseable	Rating	5% degradation (°C)	10% degradation (°C)	Tg (°C)
BF-01	BPA/BPF	5	yes	1	492	501	155
BF-02	BPA/BPF	15	yes	2c	489	506	155
BF-03	BPA/BPF	10	yes	2a	487	502	152
BF-04	BPA/BPF	5	yes	2c	508	516	153
BF-05	BPA/BPF	10	yes	3b	486	493	157
MP-HPB-01	m-HPB/p-HPB/BPF	5	yes	2a	486	495	138
MP-HPB-02	m-HPB/p-HPB/BPF	0	yes	2a	493	499	137
MP-HPB-03	m-HPB/p-HPB/BPF	10	yes	2c	488	493	138
MP-HPB-04	m-HPB/p-HPB/BPF	0	yes	2a	495	502	134
MP-HPB-05	m-HPB/p-HPB/BPF	15	yes	2b	482	491	138
MP-HPB-06	m-HPB/p-HPB/BPF	5	yes	4b	488	497	138
L-MP-HPB-01	m-HPB/p-HPB/BPF	0	yes	4b	483	494	140
L-MP-HPB-02	m-HPB/p-HPB/BPF	5	no	5	481	496	138
L-MP-HPB-02.2	m-HPB/p-HPB/BPF	5	yes	4b	494	503	136
L-MP-HPB-03	m-HPB/p-HPB/BPF	10	yes	4b	515	527	139
L-MP-HPB-03.2	m-HPB/p-HPB/BPF	10	yes	1	487	502	140
L-MP-HPB-04	m-HPB/p-HPB/BPF	15	yes	4a	492	498	139
L-MP-HPB-04.2	m-HPB/p-HPB/BPF	15	yes	2a	501	501	144
A-MP-HPB-01	m-HPB/p-HPB/BPF	5	yes	1	519	529	143
A-MP-HPB-02	m-HPB/p-HPB/BPF	10	yes	2b	505	513	141
A-MP-HPB-03	m-HPB/p-HPB/BPF	15	yes	1	515	528	142
C-MP-HPB-01	m-HPB/p-HPB/BPF	0	yes	1	195	504	139
C-MP-HPB-02	m-HPB/p-HPB/BPF	5	yes	1	495	502	142
C-MP-HPB-03	m-HPB/p-HPB/BPF	10	yes	1	491	502	143
C-MP-HPB-04	m-HPB/p-HPB/BPF	15	yes	3b	487	498	140
V-MP-HPB-04	m-HPB/p-HPB/BPF	5	yes	2a	491	503	140
V-MP-HPB-05	m-HPB/p-HPB/BPF	10	yes	1	498	505	142
V-MP-HPB-06	m-HPB/p-HPB/BPF	15	yes	2b	496	505	139
P-HPB-01	p-HBP/BPF	5	yes	4a	485	503	156

Appendix VI, Continued

P-HPB-02	p-HBP/BPF	0	yes	3b	491	497	160
P-HPB-03	p-HBP/BPF	10	yes	4a	485	492	156
P-HPB-01.2	p-HBP/BPF	5	yes	1	482	495	158
P-HPB-02.2	p-HBP/BPF	10	yes	2c	477	491	154
P-HPB-03.2	p-HBP/BPF	15	yes	2a	475	495	158
L-P-HPB-01	p-HBP/BPF	0	no	5	489	497	159
L-P-HPB-02	p-HBP/BPF	5	yes	2c	497	506	159
L-P-HPB-03	p-HBP/BPF	10	yes	3b	492	503	161
L-P-HPB-03.2	p-HBP/BPF	10	yes	3b	488	496	160
L-P-HPB-04	p-HBP/BPF	15	yes	2a	491	505	162
L-P-HPB-04.2	p-HBP/BPF	15	yes	4a	488	503	159
A-P-HPB-01	p-HBP/BPF	5	yes	3b	489	502	161
A-P-HPB-02	p-HBP/BPF	10	yes	2a	504	516	162
A-P-HPB-03	p-HBP/BPF	15	yes	3c	497	514	158
V-P-HPB-04	p-HBP/BPF	5	no	5	491	503	159
V-P-HPB-05	p-HBP/BPF	10	no	5	495	506	162
V-P-HPB-06	p-HBP/BPF	15	yes	2b	489	501	161
C-P-HPB-01	p-HBP/BPF	0	yes	1	480	493	159
C-P-HPB-02	p-HBP/BPF	5	yes	1	493	503	164
C-P-HPB-03	p-HBP/BPF	10	yes	2b	495	502	162
C-P-HPB-04	p-HBP/BPF	15	yes	4b	487	498	164
L-M-HPB-01	m-HPB/p-HPB/BPF	0	yes	2a	490	502	125
L-M-HPB-02	m-HPB/p-HPB/BPF	5	yes	4b	494	503	122
L-M-HPB-03	m-HPB/p-HPB/BPF	10	no	5	491	502	125
L-M-HPB-04	m-HPB/p-HPB/BPF	15	no	5	498	500	124
E-M-HPB-01	m-HPB/p-HPB/BPF	0	yes	3b	491	501	123
E-M-HPB-02	m-HPB/p-HPB/BPF	5	yes	1	494	503	124
E-M-HPB-03	m-HPB/p-HPB/BPF	10	yes	1	493	503	123
E-M-HPB-04	m-HPB/p-HPB/BPF	15	yes	2b	485	501	122
MIX-P-M-HPB	m-HPB/BPF, p-HPB/BPF	0	yes	1	486	498	132
MIX-MP-P-HPB	m-HPB/p-HPB/BPF, p-HPB/BPF	0	yes	2a	495	503	150
MIX-MP-M-HPB	m-HPB/p-HPB/BPF, m-HPB/BPF	0	yes	1	493	504	141

Appendix VII: Poly(arylene ether) thick samples and curing procedures

Film ID	Monomers	%Gd	Solvent	Approx. Thickness (mm)	Grams Polymer	Curing Procedure	Comments	Tg (°C)	10% Degradation (°C)
T-P-HPB-01	p-HPB/BPF	0	NMP	n/a	8.42	A	bubbled severely	159	491
T-MP-HPB-01	m-HPB/p-HPB/BPF	0	NMP	n/a	8.35	A	bubbled severely	138	481
T-MP-HPB-03	m-HPB/p-HPB/BPF	0	NMP	0.6	11.5	B	only three small bubbles	137	484
T-MP-HPB-04	m-HPB/p-HPB/BPF	0	NMP	0.6	13.02	C	no bubbles, good condition	137	501
T-MP-HPB-05	m-HPB/p-HPB/BPF	0	DMAc	n/a	13.71	D	first run- no bubbles bubbled and expanded upwords on second addition	n/a	n/a
T-MP-HPB-06	m-HPB/p-HPB/BPF	5	DMAc	n/a	23.19	C	bubbled severely; attempted to dissolve in NMP-did not dissolve	137	492
VT-P-HPB-03	p-HPB/BPF	0	NMP	1.2	13.67	C	small bubbles throughout	157	487
VT-P-HPB-04	p-HPB/BpF	5	NMP	n/a	15.52	C	bubbled severely	161	492
T-MP-HPB-07	m-HPB/p-HPB/BPF	10	DMAc	n/a	11.15	C	bubbled severely	140	486
T-MP-HPB-08	m-HPB/p-HPB/BPF	15	DMAc	n/a	10.39	C	bubbled severely	140	484
T-P-HPB-02	p-HPB/BPF	0	NMP	1.0	23.76	E	no bubbles, good condition	158	493
VT-P-HPB-05	p-HPB/BPF	5	NMP	n/a	22.05	E	bubbled severely	158	491
VT-P-HPB-06	p-HPB/BPF	10	NMP	n/a	20.19	E	bubbled severely	159	493
VT-P-HPB-07	p-HPB/BPF	15	NMP	n/a	20.87	E	bubbled severely	158	485

Appendix VII, Continued

T-M-HPB-01	m-HPB/BPF	5	NMP	n/a	18.65	E	bubbled severely; attempted to dissolve in NMP-did not dissolve	n/a	n/a
T-M-HPB-02	m-HPB/BPF	10	NMP	n/a	16.78	E	bubbled severely; attempted to dissolve in NMP-did not dissolve	n/a	n/a
T-M-HPB-03	m-HPB/BPF	15	NMP	n/a	16.35	E	bubbled severely; attempted to dissolve in NMP-did not dissolve	n/a	n/a
VT-MP-HPB-	m-HPB/p-HPB/BPF	0	NMP	1.1	12.3	F	no bubbles, good condition	140	498
VT-MP-HPB-	m-HPB/p-HPB/BPF	5	NMP	2.1	17.83	F	small bubbles	138	490
VT-MP-HPB-	m-HPB/p-HPB/BPF	10	NMP	1.6	22.63	F	small bubbles throughout	138	484
VT-MP-HPB-	m-HPB/p-HPB/BPF	15	NMP	1.5	18.72	F	small bubbles throughout	141	491
S-MP-HPB-01	m-HPB/p-HPB/BPF	0	NMP	1.7	20.78	G	two small bubbles, phase separation present	119	497
VT-M-HPB-01	m-HPB/BPF	0	NMP	2.0	17.87	G	bubbled moderately, phase separation present	117	493
AG-M-HPB-	m-HPB/BPF	5	NMP	1.4	20.83	G	no bubbles, severe phase separation	116	496
AG-M-HPB-	m-HPB/BPF	10	NMP	1.0	18.07	G	few bubbles, phase separation present	110	493
AG-M-HPB-	m-HPB/BPF	15	NMP	1.8	20.84	G	no bubbles, severe phase separation	114	486

Appendix VII, Continued

G-M-HPB-01	m-HPB/BPF	0	NMP	1.2	3.12	G	no bubbles, phase separation present	114	n/a
G-M-HPB-02	m-HPB/BPF	5	NMP	1.1	3.09	G	no bubbles, phase separation present	113	n/a
G-M-HPB-03	m-HPB/BPF	10	NMP	1.5	3.24	G	no bubbles, severe phase separation	116	n/a
AL-M-HPB-03	m-HPB/BPF	10	NMP	1.4	3	G	few bubbles	115	n/a
G-M-HPB-04	m-HPB/BPF	15	NMP	1.9	3.2	G	few bubbles, phase separation present	116	n/a
G-P-HPB-03	p-HPB/BPF	10	NMP	1.0	3.16	G	no bubbles, good condition	154	499
G-P-HPB-03.2	p-HPB/BPF	10	NMP	1.1	3.19	G	no bubbles, good condition	157	502
VT-P-HPB-01	p-HPB/BPF	0	NMP		22.7	H	one bubble, good condition	n/a	n/a

Curing Procedures

A	dry box: 1 week; oven program: ramp 100C 4hr, hold 100 4hr, ramp 200 C 4 hr, hold 4 hr, ramp 300 1 hr, hold 1 hr
B	dry box: 1 week; oven program: ramp 100C 8hr, hold 100 8hr, ramp 200 C 8 hr, hold 8 hr, ramp 300 8 hr, hold 8 hr
C	dry box: 2 weeks; oven program: ramp 100C 8hr, hold 100 8hr, ramp 200 C 8 hr, hold 8 hr, ramp 300 8 hr, hold 8 hr
D	dry box: 1 week; oven program: ramp 100C 8hr, hold 100 8hr, ramp 200 C 8 hr, hold 8 hr, ramp 300 8 hr, hold 8 hr.; poured another polymer solution once cured; repeated process
E	dry box: 2 weeks; oven program: ramp 100C 12hr, hold 100 12hr,ramp 150 12 hr, hold 12 hr ramp 200 C 12 hr, hold 12 hr, 300 12 hr, hold 12 hr
F	dry box: 3 weeks; oven held at 85 C: 3 days; oven program (ran nitrogen in oven instead of air, however, nitrogen ran out mid curing): 1day 100C-140C, 1 day 140-160C, 1day 160-180C, 1day 180-200C, 1 day 200-250C
G	heated polymer solution to 280C before pouring sample; curing process E without nitrogen running out
H	same process as H, kept sample covered with a large petri dish propped open

Appendix IX: Poly(arylene ether) viscosity data

L-P-HPB-01	Shear Rate (RPM)	3.0	2.5	3.0	2.5	2.0	1.5	0.6
0% Gd	Viscosity (cP)	7430	7420	7400	7440	7460	7420	7250

L-P-HPB-02	Shear Rate (RPM)	5.0	4.0	3.0	2.5	2.0	1.0	1.5
5% Gd	Viscosity (cP)	6940	6940	6940	6930	6940	6900	6860

L-P-HPB-03	Shear Rate (RPM)	3.0	2.5	3.0	2.5	2.0	1.5	0.6
10%Gd	Viscosity (cP)	7520	7490	7450	7470	7460	7400	7320

L-P-HPB-04	Shear Rate (RPM)	5.0	4.0	3.0	2.5	2.0	1.0	1.5
15% Gd	Viscosity (cP)	6980	6930	6950	6920	6920	6870	6830

P-HPB- Incomplete Polymerization	Shear Rate (RPM)	6.0	5.0	4.0	3.0	2.5	2.0	1.0
Pure	Viscosity (cP)	384	372	369	367	367	366	367

Appendix X: Tensile Testing Data

Film ID	% Gd	Max. Load (N)	Elastic Modulus (N/m)
MIX-MP-P	0	37	118000
MIX-MP-P	0	40	125000
MIX-MP-M	0	45	152000
MIX-MP-M	0	41	140000
MIX-MP-M	0	37	126000
MIX-M-P	0	37	139000
S-P-HPB-01	0	45	172000
S-P-HPB-02	5	37	134000
S-P-HPB-02	5	32	131000
S-P-HPB-03	10	36	142000
S-P-HPB-03	10	41	162000
S-P-HPB-04	15	53	244000
S-P-HPB-04	15	54	234000
S-P-HPB-04	15	53	218000
S-P-HPB-04	15	40	185000
E-M-HPB-02	5	44	234000
E-M-HPB-02	5	37	197000
BF-01	5	45	118000
BF-01	5	45	156000
BF-01	5	44	155000
BF-01	5	44	149000
BF-01	5	46	163000
BF-03	10	40	155000
Kapton	0	44	88000
Kapton	0	41	97000
Kapton	0	47	100000
Kapton	0	44	92000
Kapton	0	48	94000
Kapton	0	44	94000

Appendix XI: Poly(arylene ether) X-ray absorption data

Film ID	% Gd	3x3 Inch Thickness (mm)	% X-Rays Absorbed	2Th (°)
BF-01	5	0.058	10	27.90
BF-04	5	0.062	11	18.58
BF-05	10	0.069	19	27.9
BF-03	10	0.069	17	18.58
BF-02	15	0.06	25	27.9
MP-HPB-04	0	0.036	2	18.58
MP-HPB-02	0	0.037	2	18.58
C-MP-HPB-01	0	0.091	5	27.90
MP-HPB-01	5	0.043	9	18.58
MP-HPB-06	5	0.073	13	18.58
A-MP-HPB-01	5	0.055	10	27.90
V-MP-HPB-04	5	0.042	5	27.90
C-MP-HPB-02	5	0.081	14	27.90
MP-HPB-03	10	0.04	11	18.58
V-MP-HPB-05	10	0.055	12	27.90
L-MP-HPB-03.2	10	0.069	18	18.58
C-MP-HPB-03	10	0.086	24	18.58
MP-HPB-05	15	0.038	16	18.58
A-MP-HPB-03	15	0.063	24	27.90
V-MP-HPB-06	15	0.056	22	27.90
L-MP-HPB-04.2	15	0.067	26	18.58
C-MP-HPB-04	15	0.096	33	27.90
P-HPB-02	0	0.06	1	18.58
C-P-HPB-03	0	0.035	2	27.90
P-HPB-01	5	0.067	9	18.58
L-P-HPB-02	5	0.067	10	27.90
L-P-HPB0-3.2	10	0.071	17	18.58
L-P-HPB-04	15	0.052	21	18.58
P-HPB-03.2	15	0.07	27	18.58
L-M-HPB-01	0	0.065	3	27.90
E-M-HPB-01	0	0.091	3	27.90
E-M-HPB-02	5	0.048	8	27.90
E-M-HPB-03	10	0.051	13	27.90
E-M-HPB-04	15	0.064	22	27.90

Appendix XII: Poly(arylene ether) x-ray absorption Beer's Law Analysis Graphs

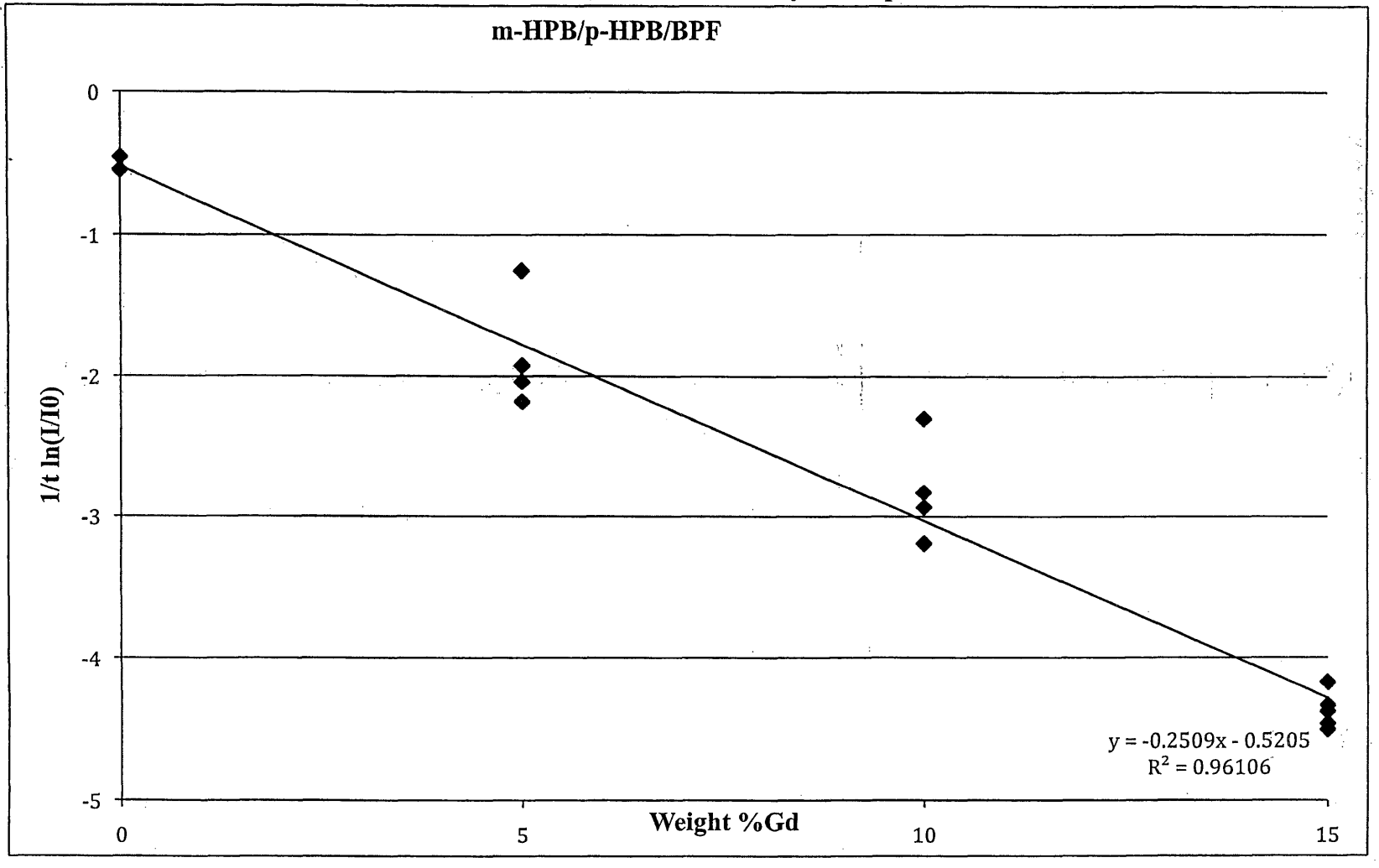

Appendix X, Continued

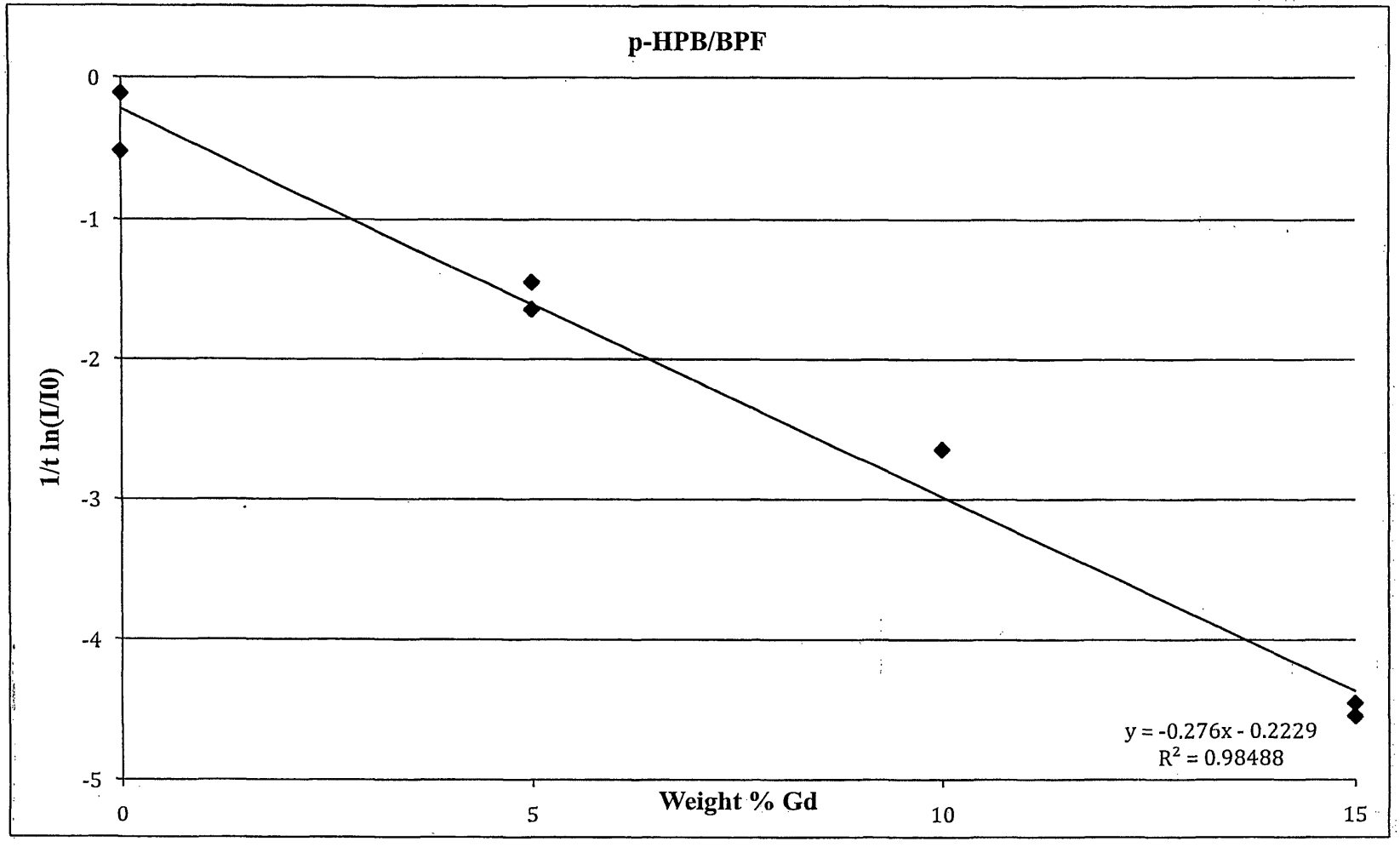

Appendix X, Continued

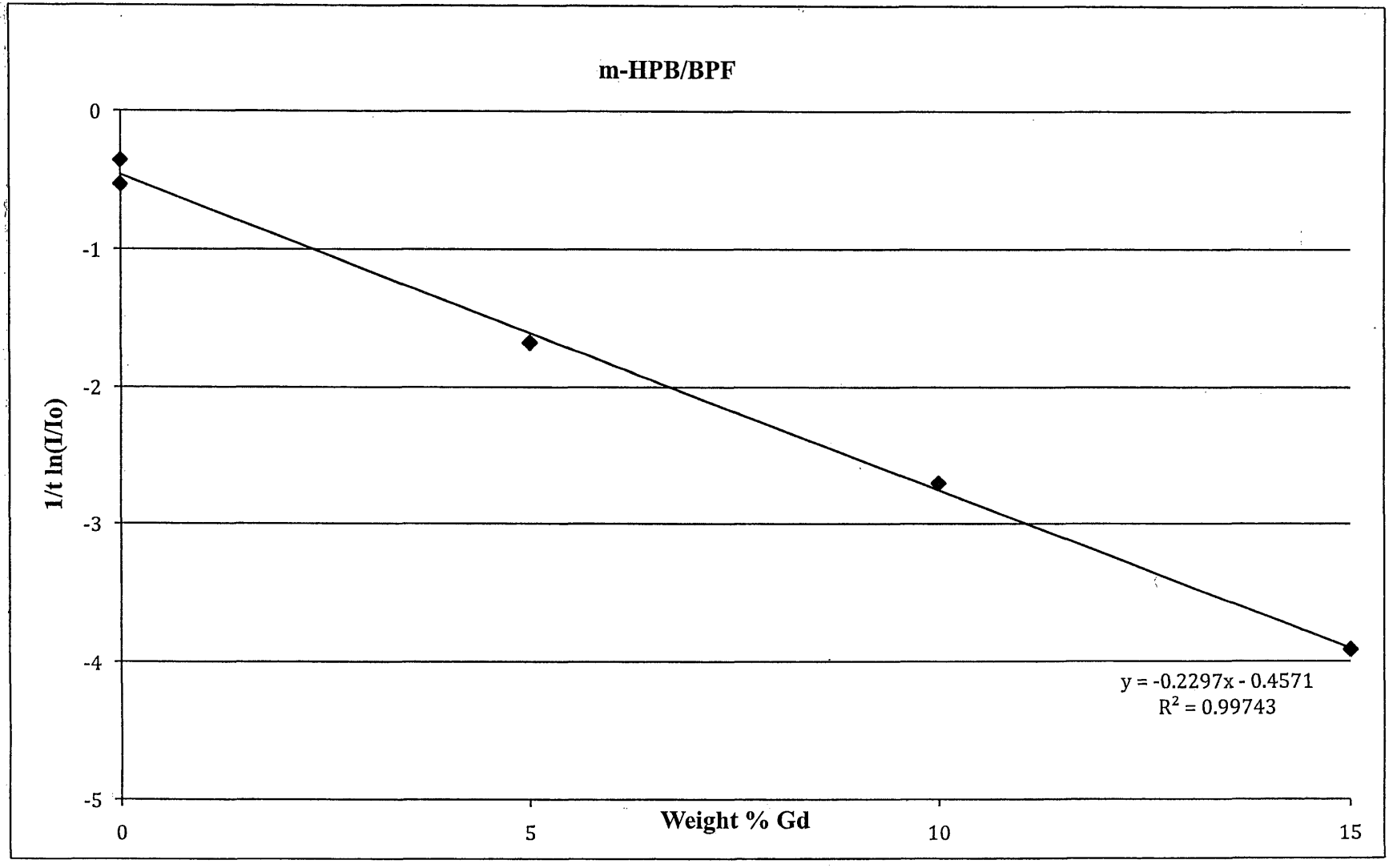

Appendix X, Continued

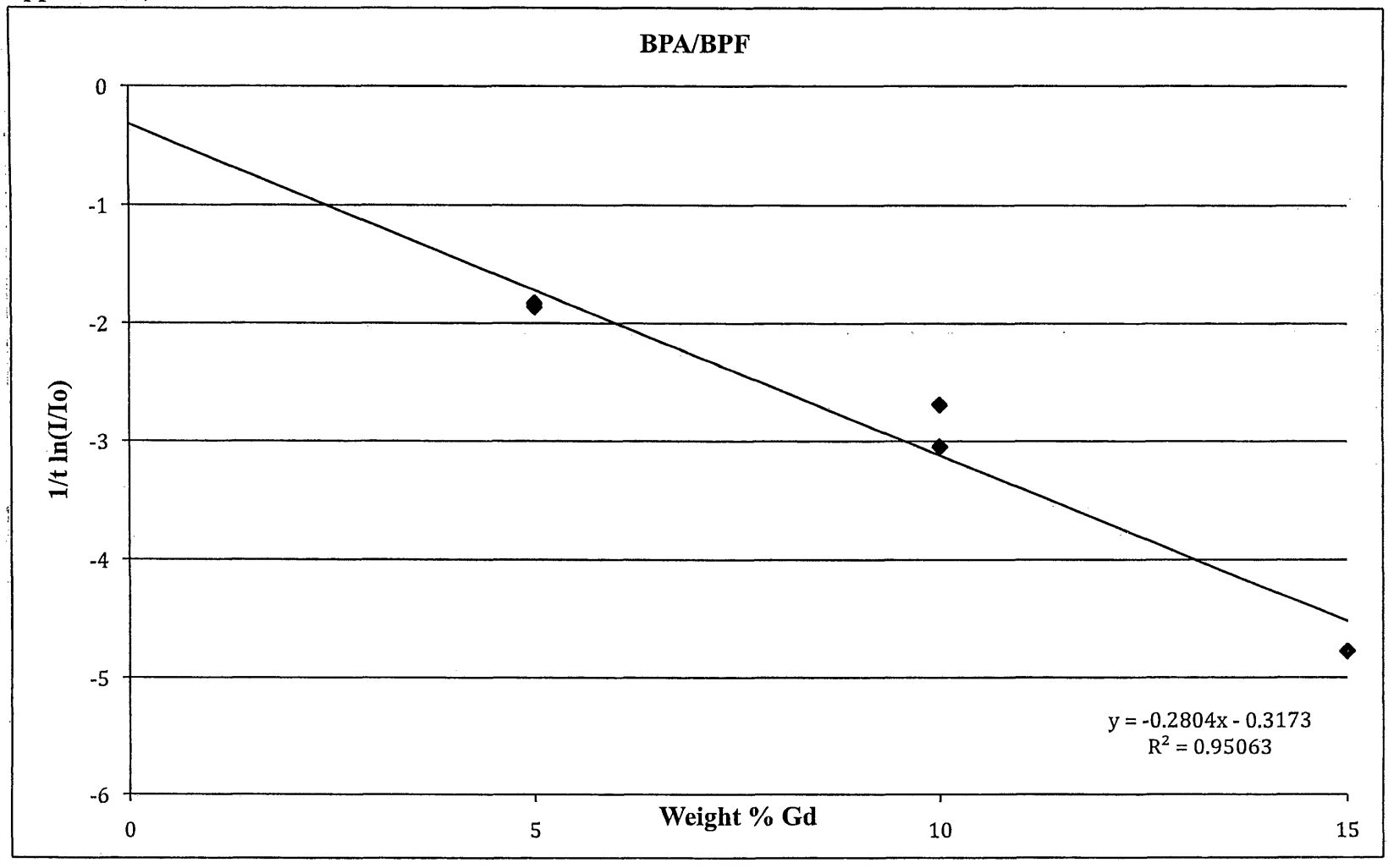

Appendix XIII: Neutron absorption testing data

Sample Type	%Gd	Thickness (mm)	A_0	% Neutrons Absorbed
p-HPB/BPF	0	0.048	3826	1
p-HPB/BPF	5	0.054	3665	5
p-HPB/BPF	10	0.059	3497	10
p-HPB/BPF	15	0.063	3517	9
p-HPB/BPF	15	0.091	3659	5
m-HPB/BPF	0	0.056	3879	0
m-HPB/BPF	5	0.062	3683	5
m-HPB/BPF	10	0.052	3646	6
m-HPB/BPF	15	0.067	3498	10
m-HPB/p-HPB/BPF	0	0.042	3847	0
m-HPB/p-HPB/BPF	5	0.045	3766	3
m-HPB/p-HPB/BPF	10	0.047	3630	6
m-HPB/p-HPB/BPF	15	0.049	3824	1
m-HPB/p-HPB/BPF	15	0.059	3519	9
Indium Foil	n/a	2	3866	n/a

Appendix XIV: Poly(arylene ether) neutron absorption Beer's law analysis graphs

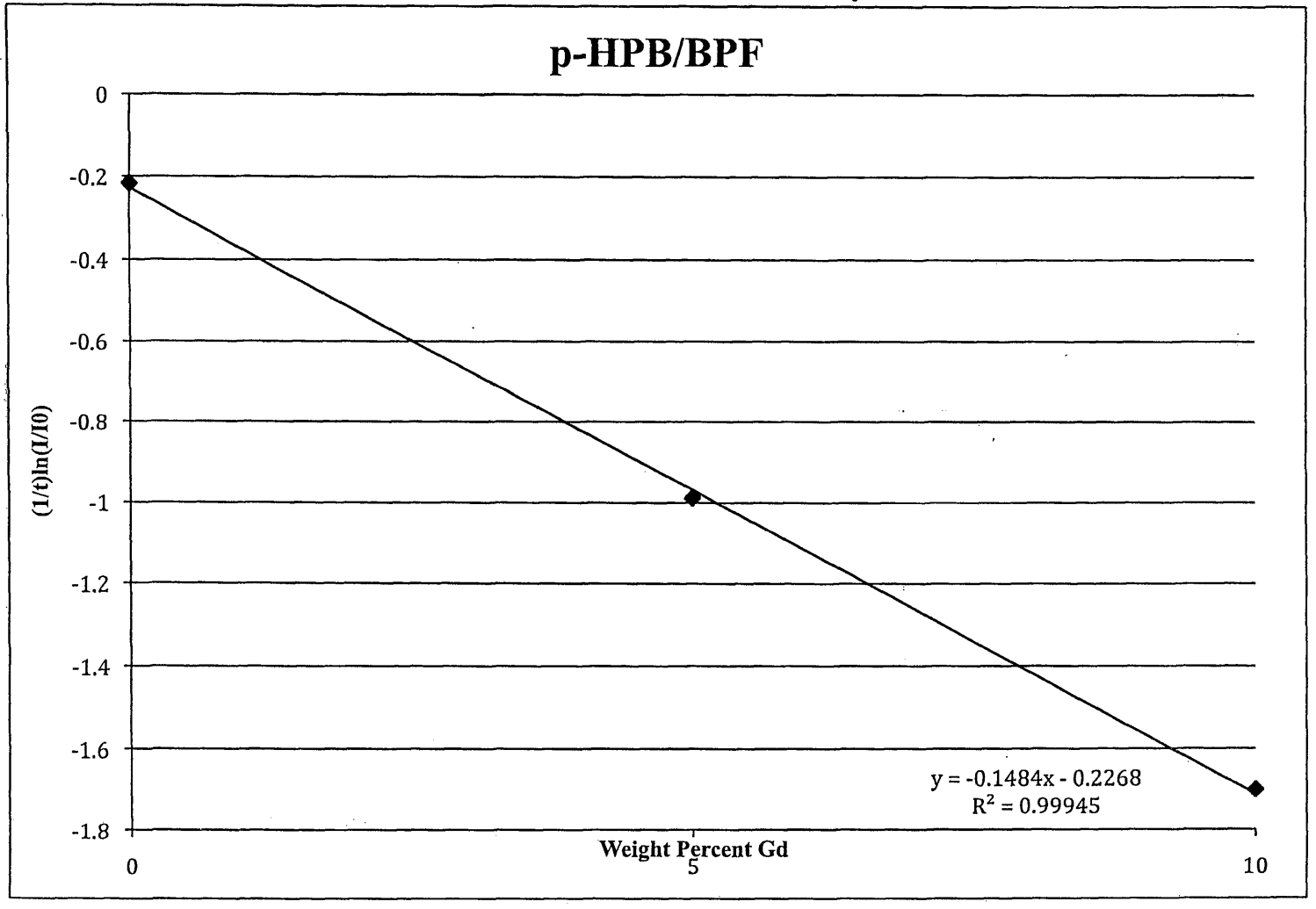

Appendix XII: Poly(arylene ether) neutron absorption Beer's law analysis graphs

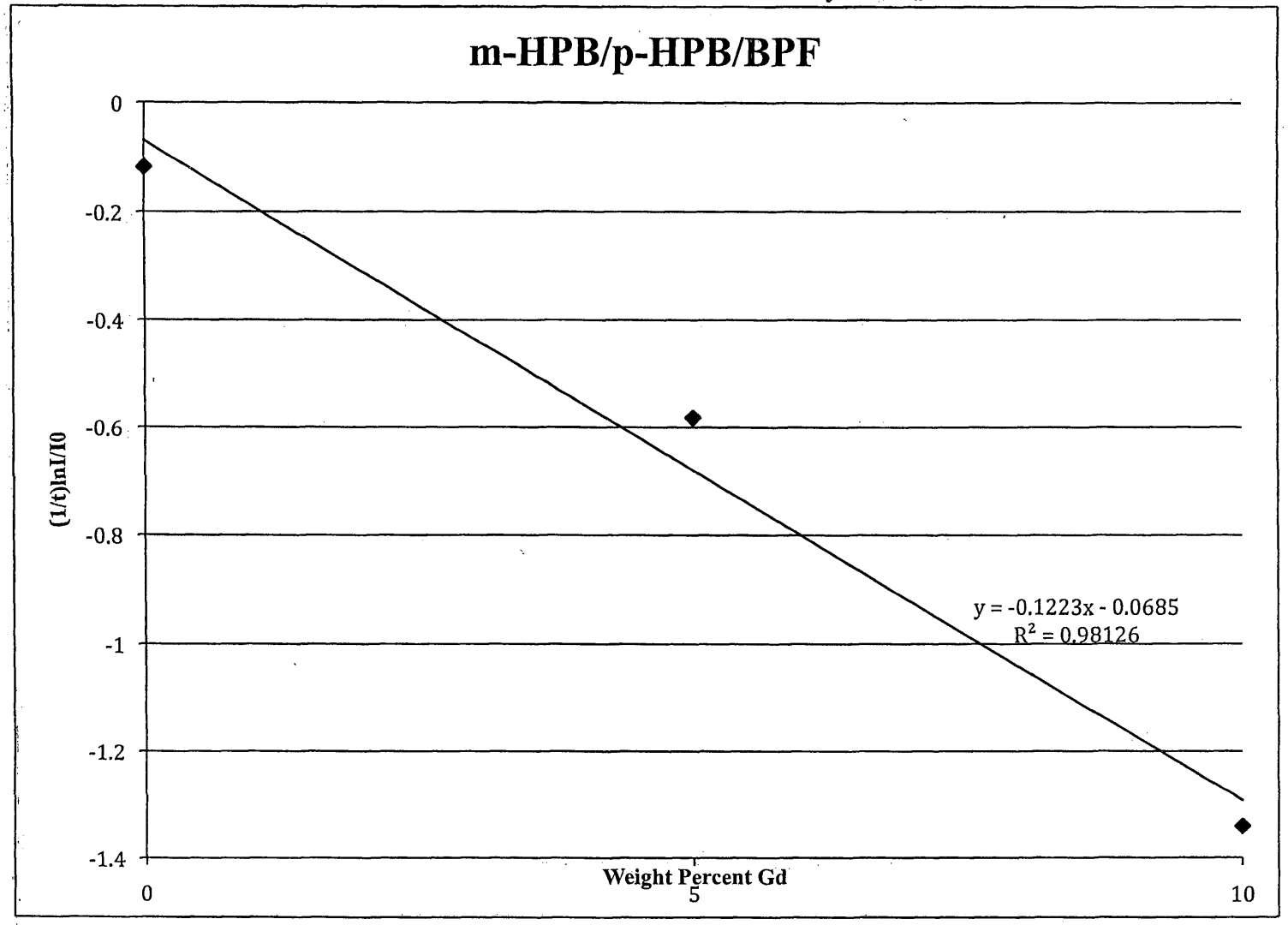

Appendix XII: Poly(arylene ether) neutron absorption Beer's law analysis graphs

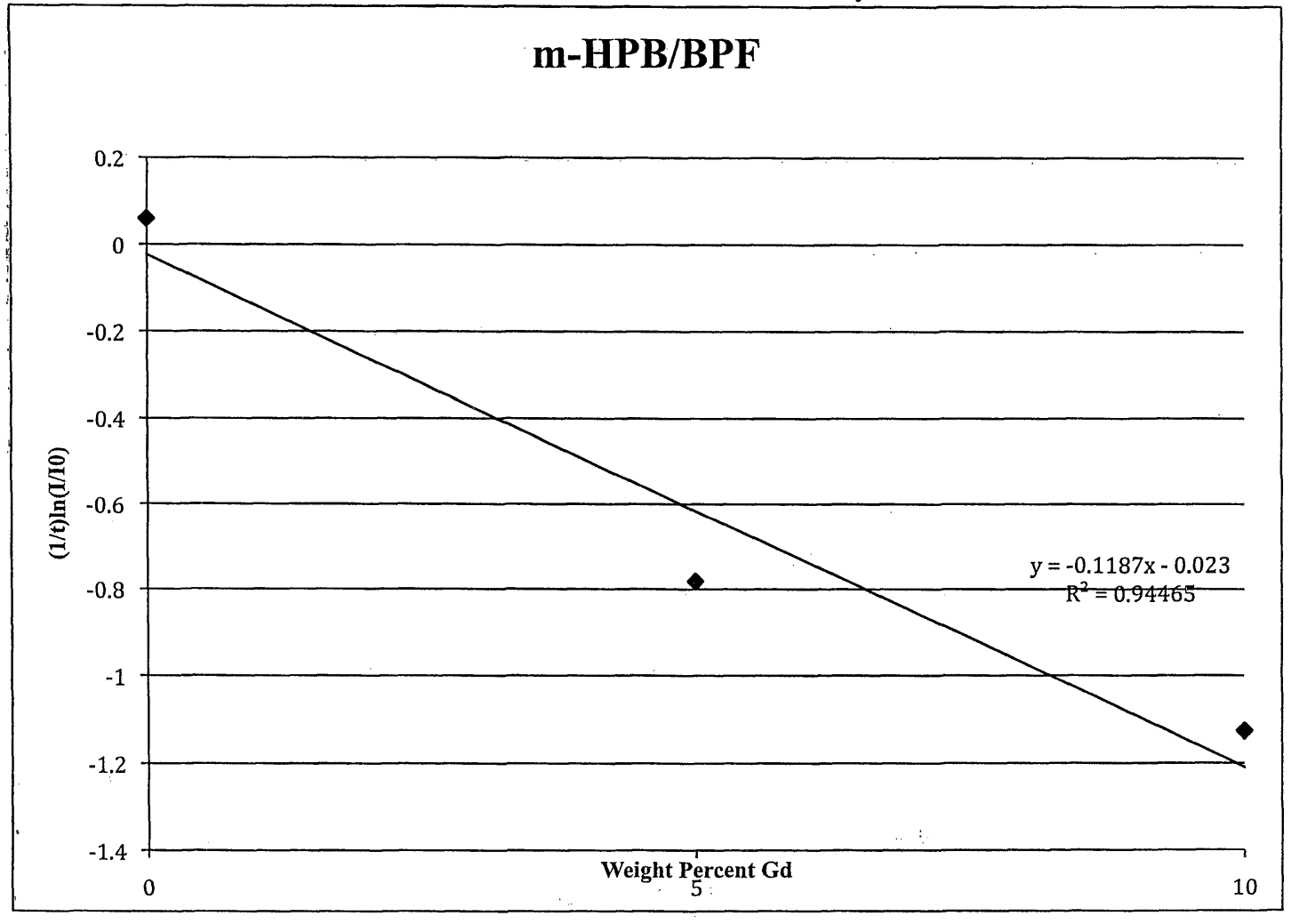

Appendix XV: TGA of gadolinium phenylacetate

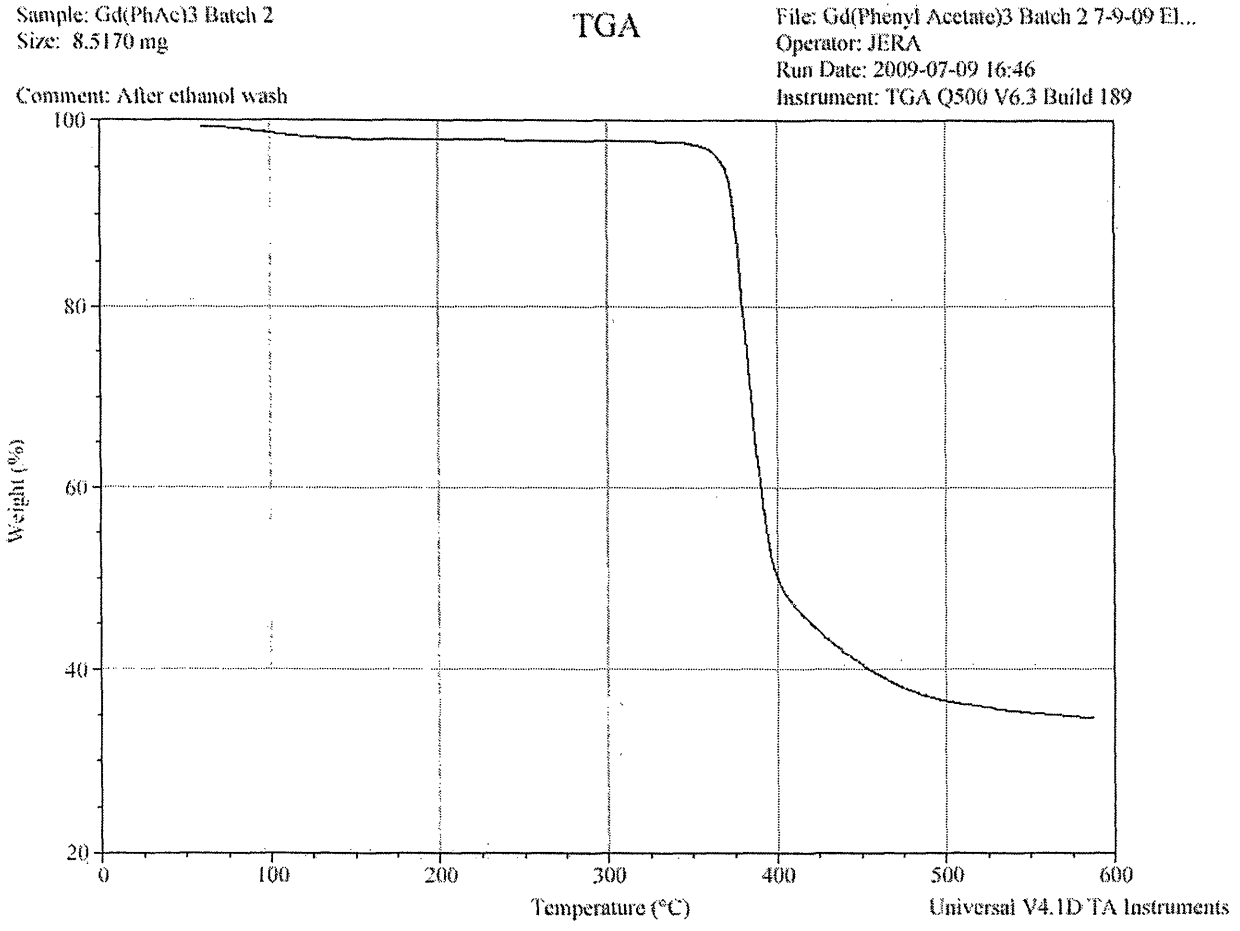

VITA

Emily Grace Harbert is a master of science candidate in Chemistry at The College of William and Mary specializing in polymer science. She received her Bachelor of Science, cum laude, with High Honors in Chemistry Research, in 2008 from The College of William and Mary. Her master's thesis, "Multifunctional Polymer Synthesis and Incorporation of Gadolinium Compounds and Modified Tungsten Nanoparticles for Improvement of Radiation Shielding for Use in Outer Space," focuses on the design and development of new polymers with enhanced radiation shielding capabilities to protect humans for extended space exploration.